DOI:
10.1152/ajpheart.00218.2019
10.1152/ajpheart.00218.2019

Document Version
Peer reviewed version

Modelling arterial pulse waves in healthy ageing: a database for in silico evaluation of haemodynamics and pulse wave indices

Peter H. Charlton [1], Jorge Mariscal-Harana [1], Samuel Vennin [1,2], Ye Li [2], Phil Chowienczyk [2], Jordi Alastruey [1,3]

[1] Department of Biomedical Engineering, School of Biomedical Engineering and Imaging Sciences, King's College London, King's Health Partners, London, SE1 7EH, UK

[2] Department of Clinical Pharmacology, King's College London, King's Health Partners, London, SE1 7EH, UK

[3] Institute of Personalized Medicine, Sechenov University, Moscow, Russia

Abbreviated Title: Modelling arterial pulse waves in healthy ageing

Corresponding Author: Peter H. Charlton peter.charlton@kcl.ac.uk

Department of Biomedical Engineering, 4th Floor Lambeth Wing, St Thomas' Hospital, Westminster Bridge Road, London, SE1 7EH

Abstract

The arterial pulse wave (PW) is a rich source of information on cardiovascular (CV) health. It is widely measured by both consumer and clinical devices. However, the physical determinants of the PW are not yet fully understood, and the development of PW analysis algorithms is limited by a lack of PW datasets containing reference CV measurements. Our aim was to create a database of PWs simulated by a computer to span a range of CV conditions, representative of a sample of healthy adults. The typical CV properties of 25-75 year olds were identified through a literature review. These were used as inputs to a computational model to simulate PWs for subjects of each age decade. Pressure, flow velocity, luminal area and photoplethysmographic (PPG) PWs were simulated at common measurement sites, and PW indices were extracted. The database, containing PWs from 4,374 virtual subjects, was verified by comparing the simulated PWs and derived indices with corresponding *in vivo* data. Good agreement was observed, with well-reproduced age-related changes in haemodynamic parameters and PW morphology. The utility of the database was demonstrated through case studies providing novel haemodynamic insights, *in silico* assessment of PW algorithms, and pilot data to inform the design of clinical PW algorithm assessments. In conclusion, the publicly available PW database (DOI: 10.5281/zenodo.2633175) is a valuable resource for understanding CV determinants of PWs, and for the development and pre-clinical assessment of PW analysis algorithms. It is particularly useful because the exact CV properties which generated each PW are known.

41 **New & Noteworthy**

42 Firstly, a comprehensive literature review of changes in CV properties with age was
43 performed. Secondly, an approach for simulating PWs at different ages was designed and verified
44 against *in vivo* data. Thirdly, a PW database was created, and its utility was illustrated through three
45 case studies investigating the determinants of PW indices. Fourthly, the database, and tools for
46 creating the database, analysing PWs, and replicating the case studies, are freely available.

47

48 **Key terms**

49 arteries; pulse wave; ageing; database of virtual subjects; blood flow

50

51

1 Introduction

The arterial pulse wave is used for physiological assessment in both clinical medicine and consumer devices. The pulse wave (PW) contains a wealth of information on the cardiovascular system (4). It is influenced by the heart, with properties such as heart rate and stroke volume influencing its duration and morphology, and the vasculature, with arterial stiffness and wave reflections influencing its morphology. Consequently, a range of physiological parameters can be estimated from the PW, which are useful for diagnosis, monitoring and clinical decision making. The PW can be easily measured using non-invasive clinical devices, such as oscillometric blood pressure monitors and pulse oximeters. It is also routinely monitored by consumer devices such as smart watches and fitness wristbands (27). As a result, there is scope for obtaining great insight into cardiovascular function from the PW in clinical settings and daily life.

The PW has been the subject of much *in vivo* research. For instance, the physiological determinants of pulse wave velocity (PWV) and late systolic pressure augmentation have been investigated in both large observational studies (98) (37) and smaller interventional studies (106) (168). In addition, techniques for estimating physiological parameters from PWs have been assessed in clinical studies, including: estimating cardiac output from invasive pressure PWs (153); estimating arterial stiffness from non-invasive pressure PWs (69); and, estimating an aortic pressure wave from a peripheral PW (117). Whilst *in vivo* studies are valuable they do have disadvantages, as described in (171): it can be difficult to measure reference variables precisely (*e.g.* cardiac output or arterial stiffness); it is difficult to study the influence of individual cardiovascular properties on the PW in vivo, since other properties may change concurrently; it can be difficult to measure PWs at all sites of interest (particularly central arteries); clinical trials are expensive and time-consuming; and, *in vivo* measurements are subject to experimental error.

One-dimensional (1D) computational modelling provides a complementary approach for research into the PW, as it allows PWs to be simulated under different cardiovascular conditions (146). Indeed, *in silico* studies using computational modelling have been performed to complement the aforementioned clinical studies: the determinants of PWV and pressure augmentation were assessed in (170) (171), and techniques for estimating cardiac output, arterial stiffness, and the aortic pressure wave, were assessed in (116) (157) (151). Whilst there are also disadvantages to *in silico* studies (*e.g.* reliance on modelling hypotheses), they can provide additional haemodynamic insights which would be difficult to obtain *in vivo*, and can be used for preliminary design and assessment of PW analysis techniques across a wide range of cardiovascular conditions in a relatively quick and inexpensive manner. Furthermore, the results of *in silico* studies can be used to inform the design of *in vivo* studies (171), and to confirm the findings of *in vivo* studies (90, 161).

The aim of this study is to develop and verify an approach for simulating PWs representative of a sample of healthy adults. Such an approach would be useful for *in silico* studies of haemodynamics and PW indices, as the results could be indicative of those which would be obtained *in vivo*. The approach presented here combines novel methods with several recent developments in 1D modelling from the literature. The main goals were to: (i) develop methods for simulating PWs during healthy ageing, exhibiting normal physiological variation; (ii) develop a method for simulating photoplethysmogram (PPG) PWs, which are widely measured by pulse oximeters and consumer devices; (iii) create a database of PWs representative of a sample from a healthy adult population, and verify it through comparison with *in vivo* data; (iv) present case studies demonstrating the utility of the approach; and (v) make the PW database and accompanying code freely available to support further research. This builds on preliminary work presented in (23, 24, 31, 34).

2 Materials and Methods

2.1 Modelling Arterial Pulse Waves

The 1D formulation of PW propagation was used to simulate arterial PWs numerically (108). The computational model was based on that described in (2). It consisted of three key components, as shown in Figure 1. Firstly, the arterial network was decomposed into 116 arterial segments making up the larger arteries of the thorax, limbs and head. Arterial segments were modelled as thin, visco-elastic tubes of constant length and linearly tapered diameter (30). Secondly, a periodic inflow waveform was prescribed as a boundary condition at the aortic root, modelling flow from the left ventricle. Thirdly, terminal 3-element Windkessel boundary conditions were imposed at the outlets of peripheral arterial segments, modelling vascular beds.

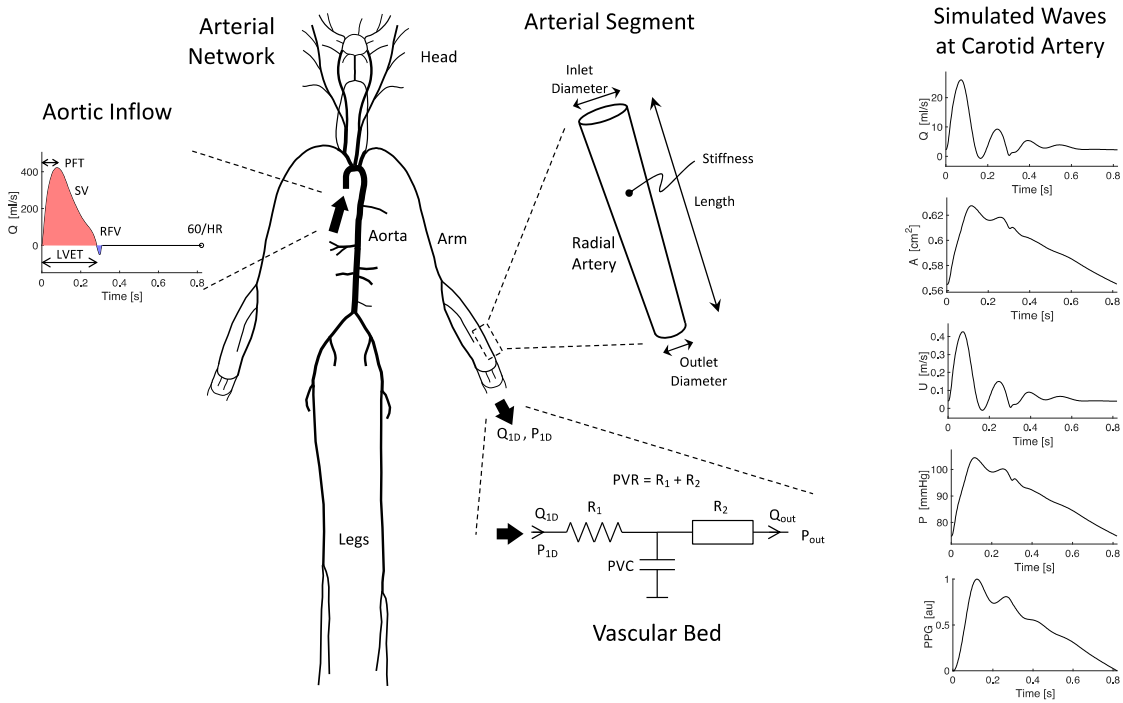

Figure 1: The 1D model of pulse wave propagation (left) and simulated pulse waves (right). The model consists of: an arterial network consisting of arterial segments making up the larger arteries; an aortic

112 inflow waveform prescribed at the aortic root; and lumped boundary conditions at each terminal
113 segment representing vascular beds (adapted from (30) [CC BY 3.0]).

114 The nonlinear 1D equations of incompressible and axisymmetric flow in Voigt-type visco-
115 elastic vessels were used to model blood flow, based on the physical principles of conservation of
116 mass, momentum and energy (30). Key assumptions were: laminar flow, incompressible and
117 Newtonian blood (density, ρ = 1,060 kg/m^3, and viscosity, μ = 2.5 mPa.s), parabolic flow and no
118 energy losses at bifurcations. The previously described model provided four types of arterial PWs:
119 blood flow velocity (U), luminal area (A), volume flow rate ($Q = UA$), and blood pressure (P) waves. In
120 this study the model was extended to simulate photoplethysmogram (PPG) PWs by assuming that
121 the PPG is dependent on the volume of arterial blood in a tissue. At the periphery, the PPG PW was
122 calculated from the volume of blood stored in the terminal Windkessel model. Within the arterial
123 network the PPG was calculated from the volume of blood stored in the arterial segment. In both
124 cases the PPG was calculated by normalising the pulsatile variation in blood volume to occupy a
125 range of 0 to 1.

126 For further details of the model, including the geometry of the arterial network and the
127 methodology for simulating PPG PWs, see Appendix, Section 5.1.

128

129 **2.2 Prescribing Model Input Parameters for Different Ages Based on a Literature Review**

130 The model input parameters were adjusted to simulate PWs representative of healthy adults
131 at each age decade from 25 to 75 years. The parameters can be categorised as: cardiac, arterial,
132 vascular bed, and blood properties. Referring to Figure 1: the cardiac properties influence the aortic
133 inflow waveform; the arterial properties determine the mechanical and geometrical characteristics
134 of arterial segments; and the vascular bed properties are captured by the components of the
135 vascular bed model. In this section we present a review of the literature describing changes in these
136 properties with age, including findings from 97 articles, and describe the methods used to extract

137 values for the mean and inter-subject variation of each model input parameter at each age decade.
138 The findings for each parameter are presented in the Appendix, Section 5.2. The most reliable
139 studies reporting the mean and inter-subject variation of each parameter at each age were
140 identified using the following criteria: (i) whether the reported change with age was in keeping with
141 the consensus from the review; (ii) the accuracy of the technique used to measure the parameter;
142 and (iii) the nature of the subjects studied (namely their level of health, age range and sample size).

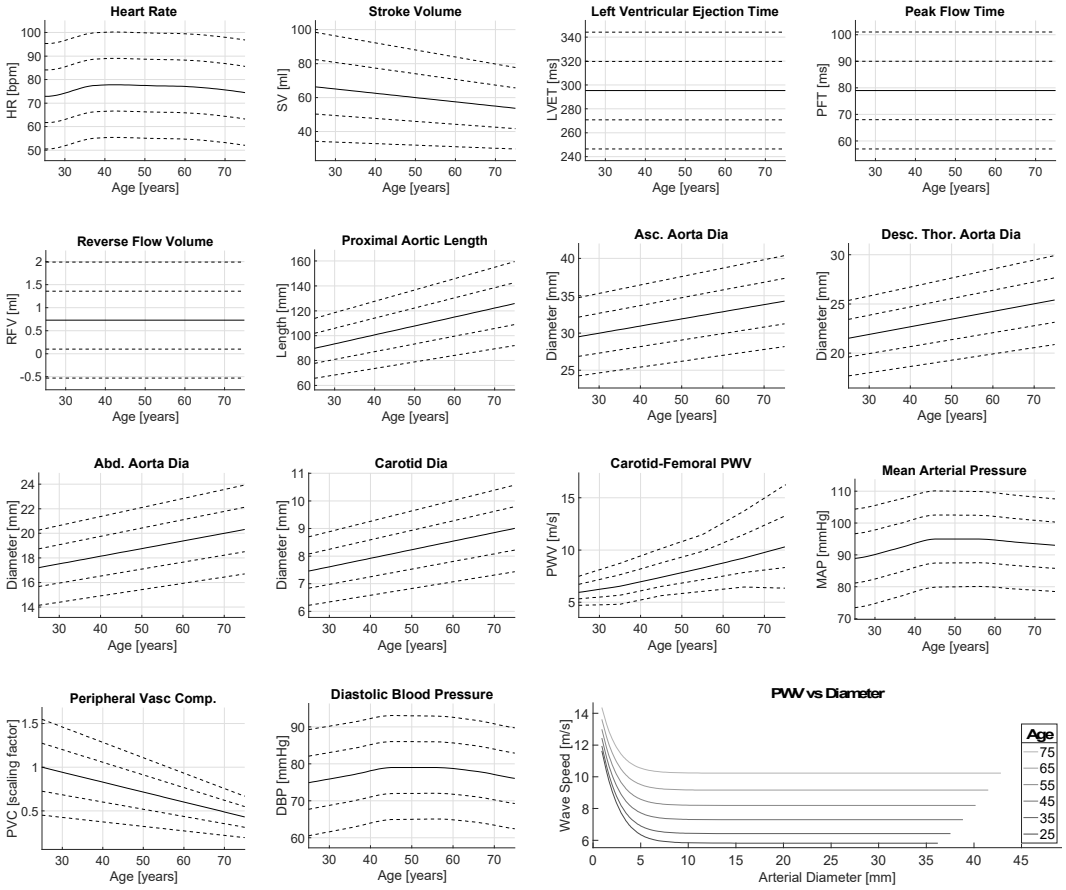

Figure 2: A summary of the literature review findings. The mean (solid line) and standard deviation (dashed lines indicating $\pm$ 1 and $\pm$ 2 SD) values are shown for each parameter. The positive and negative SD values for carotid-femoral PWVs are different to capture the positive skewness of this variable's distribution. The final wave speed plot shows the baseline wave speed as a function of diameter for each age.

143 The typical values found for a sample of healthy adults are shown for each parameter in Figure 2,
144 and the equations describing them as a function of age are provided in the Appendix, Section 5.2.

145 **2.2.1 Cardiac Properties**

146 Cardiac properties were specified to the model through an inflow waveform prescribed at
147 the aortic root (shown in Figure 1). The waveform is affected by: heart rate (HR), stroke volume (SV),
148 left ventricular ejection time (LVET), peak flow time (PFT), reverse flow volume (RFV), and aortic flow
149 waveform morphology. These characteristics are now considered in turn.

150 The vast majority of the identified articles which investigated changes in HR with age (7, 15,
151 36, 45, 54, 70, 83, 96, 103, 104, 109, 122, 125, 128, 129, 132, 133, 137, 142, 148, 174, 175) did not
152 find a change with age (see Table A1). (174) reported a nonlinear change in HR between the ages of
153 28 and 90 in Framingham Heart Study data (n=5,209): an increase until around 55 years in males,
154 followed by a slight decrease until age 70, and a rapid decline thereafter. The change observed in
155 this study was small, with the mean HR varying between 67 and 76 beats per minute (bpm) for
156 males. When combined with the nonlinear nature of the change, and the inclusion of older subjects
157 in this study, this may explain why most other studies did not identify a change. This study was used
158 to model changes in HR with age since it was population-based and far larger than the others. Mean
159 values for each age were obtained by interpolating the male data from this study using shape-
160 preserving piecewise cubic interpolation. Values for normal variation in HR were not provided by this
161 paper. Therefore, a standard deviation of 11 bpm was obtained from a population study of 800 UK
162 Biobank participants aged 45-74 years old (119). It was assumed that this value remained constant
163 with age. The HR was prescribed to the model by setting the duration of the inflow waveform,
164 $T = 60/HR$.

165 The majority of the identified articles (20, 22, 70, 89, 103, 109, 119, 121, 122, 132, 133)
166 indicated that SV decreases with age. The largest study was an analysis of echocardiographic data

acquired from 3,719 subjects (121). This study was chosen to model both the change in SV with age, and normal variation in SV. The mean and standard deviation values for SV at each age were estimated from the upper and lower male reference values by assuming a normal distribution. SV was input to the model by setting the integral of the input flow waveform, *Q(t)*, as $\int_0^T Q(t)\,dt = SV$, where *t* is time and *T* is the duration of a cardiac cycle.

The majority of the identified studies (54, 55, 68, 104, 122, 125, 137, 145, 155, 172) observed no change in LVET with age. Gold standard measurement techniques (echocardiograms and Doppler aortic flow signals) were used in three studies with low numbers of subjects (83, 65 and 62 subjects), which all found no change in LVET with age (54, 55, 137). Other studies included data from over 350 subjects, but did not use gold standard measurements, instead using the duration of the systolic portion of the carotid flow or pressure signal (68, 172), the QT interval (104, 155) or phonocardiogram measurements (145). They reported a range of conclusions: no change (104, 122, 145), an increase (155), or a small nonlinear change (172). Therefore, it was assumed that LVET did not change with age. A mean value of 282 ms was obtained from (108). Although this is slightly lower than the values of 295 ± 24 and 306 ± 22 ms reported in (55, 137), it was chosen because it provided more realistic PW shapes. (55) was used to model normal variation in LVET. Several articles have reported that LVET changes with HR (49, 64, 124, 136, 138, 145, 165, 166, 172) and SV (64, 124, 165). Data on the relationship between LVET, HR and SV were reported in (166). The data from normal subjects were used to calculate an empirical relationship,

$$LVET\ [ms] = 244 - 0.926\ HR\ [bpm] + 1.08\ SV\ [ml]\,, \qquad (1)$$

which was used to model the changes in LVET with HR and SV.

There is little information in the literature on how the PFT is affected by age. A study of 82 healthy subjects aged 21 to 78 years found no significant change in PFT with age when measured with gold standard aortic Doppler flow (54). Similarly, a study of 96 healthy subjects aged 19 to 79

191 years also found no significant change (MRI measurements at ascending aorta) (15). In contrast, a
192 study of PFT estimated from carotid pressure waves in 56 healthy subjects found a substantial
193 decrease with age (68). Due to the limited and conflicting evidence, it was assumed that PFT did not
194 change with age. A normal value of 79 ± 11 ms was obtained from echocardiography data in (74).

195 The ascending aortic flow waveform typically consists of a positive systolic flow wave,
196 followed by a period of reverse flow (111). There is little information in the literature on RFV.
197 Bensalah *et al.* found no significant difference in RFV between young and elderly subjects in the
198 ascending aorta (although they did observe an increase in peak backward flow rate with age) (15).
199 Similarly, Svedlund *et al.* found no difference between the ratios of systolic to diastolic velocity time
200 integrals in the aortic arch between younger and older subjects (154). Therefore, it was assumed
201 that RFV did not change with age. A normal value of 0.73 ± 0.63 ml was obtained from ascending
202 aortic data from (15).

203 The aspects of the aortic inflow waveform considered so far can be used to specify the
204 integral of the waveform, its duration, and the timings of peak flow and end-systole. There is little
205 evidence in the literature on how the remaining aortic flow wave characteristics vary with age and
206 within age groups. Examples of aortic flow waveforms for young and old subjects are provided in
207 (109) (15) (111), although these are based on measurements from individual subjects. Therefore, it
208 was assumed that the remaining aortic flow wave characteristics did not change with age, or exhibit
209 any variation. The morphology was modelled on the wave provided in (108), since this has been
210 previously shown to give reasonable PW simulations. Details of the methodology used to prescribe
211 an inflow waveform with the desired characteristics are provided in the Appendix, Section 5.3.1.

212 **2.2.2 Arterial Properties**

213 The following properties of arterial segments were specified to the model: length, inlet and
214 outlet diameters, wall stiffness, and wall viscosity. These are now considered in turn.

215 Few studies have investigated how arterial lengths change with age. The length of the
216 proximal aorta has been found to increase with age (15, 40, 67, 152). In contrast, the lengths of
217 more distal sections of the aorta (42, 67, 152) and the carotid (152) and iliac (152) arteries have
218 been found to either not change with age, or exhibit a complex change (in one case). Therefore, it
219 was assumed that the proximal aorta (up to and including the aortic arch) lengthens with age,
220 whereas the lengths of other arteries do not change. Baseline lengths for the 25-year old were
221 adapted from those in (3, 108). Relative changes in proximal aortic length with age were modelled
222 using data from (67) since it used reliable methodology (MRI measurements of the aortic arch, 157
223 subjects, aged 18 - 77 years). However, it did not provide age-specific values for the normal variation
224 in length. Therefore, normal variation was modelled using data from (15).

225 Several studies have investigated how the diameters of the aorta (ascending (1, 15, 21, 67,
226 82, 97, 103, 109, 127, 131, 158, 162, 163), descending thoracic (1, 67, 127, 131, 162), abdominal (67,
227 73, 118, 131, 150, 162)) and carotid artery (13, 16, 63, 68, 129, 140) change with age, with the vast
228 majority indicating that both increase with age. In contrast, few studies investigated changes in the
229 diameters of the iliac (73, 118), femoral (13, 139, 140), brachial (57, 66), or radial (16) arteries, and
230 these reported a range of conclusions. Therefore, it was assumed that the diameters of the aorta
231 and carotid artery increase with age, whereas the diameters of remaining arteries are not affected
232 by age. Baseline diameters for the 25-year old were adapted from (3, 108). A study by Hickson *et al.*
233 (n=157) was used to model changes in aortic diameter with age since it contained data from all three
234 aortic sites, from subjects free of cardiovascular disease and medication, over a wide age range (24 -
235 73 years), acquired using MRI (67). However, this study did not provide data on normal variation in
236 aortic diameter. Therefore, normal variation was modelled using data from (1). Changes with age
237 and normal variation in carotid artery diameter were modelled using data from (63), since it used
238 echo-tracking measurements from healthy subjects with a wide age range. The arterial diameters

were prescribed at male age-specific diastolic blood pressure (DBP) values from (100), a study of 4,001 healthy subjects.

The literature on changes in pulse wave velocity (PWV) with age was reviewed to identify target PWVs for optimising the stiffness of arterial segments. Many studies have investigated how PWV changes with age in the aorta (9, 10, 12, 15, 56, 62, 65, 67, 81, 92, 98, 100, 103, 107, 112, 128, 143, 147, 160) and the arteries of the arms (9, 10, 18, 19, 50, 62, 65, 87, 100, 107, 149) and legs (9, 10, 43, 65, 92). The vast majority observed an increase in PWV with age. The largest study reported reference values of carotid-femoral PWV (n = 11,092) according to age and blood pressure (98). The subjects in this study were from eight European countries, free from overt cardiovascular disease, and aged from 15 to 97. Therefore, this study was used to model changes in aortic PWV with age and MAP. We found no similar population-level studies reporting how PWVs at the arm and leg change with age. Instead, relationships between aortic and brachial-radial (arm) and femoral-dorsalis pedis (leg) PWVs were calculated from the data in (9) (n = 524). These relationships were then used to calculate desired values for arm and leg PWVs corresponding to the desired aortic PWVs. Following (108, 114, 170), the stiffness of each segment was assumed to be related to its diastolic radius, R_d, using

$$Eh = R_d\,[k_1\,exp(k_2\,R_d) + k_3]\,, \qquad (2)$$

where *E* is the Young's modulus, *h* the wall thickness, and k_1, k_2 and k_3 are empirical constants which were optimised to provide theoretical wave speeds, c_d, in keeping with the desired PWVs (for further details see the Appendix, Section 5.3.2). c_d was calculated as (2)

$$c_d = \sqrt{\frac{2Eh}{3\rho R_d}}. \qquad (3)$$

Wall viscosity, Γ, was calculated following (108) as

$$\Gamma = \frac{b_1}{2R_d} + b_0 \quad (4)$$

where b_1= 150 g cm/s and b_0= 600 g/s are empirical constants, chosen to achieve realistic hysteresis in pressure-area curves at peripheral arteries. Wall viscosity was assumed to remain constant with age as there is little evidence to suggest otherwise (77).

2.2.3 Vascular Bed Properties

It is difficult to assess the properties of vascular beds *in vivo*. Therefore, we considered changes in systemic vascular properties reported in the literature, and used these to inform the expected changes in vascular bed properties.

The majority of articles describing variations in systemic vascular resistance (SVR) with age (36, 45, 70, 76, 101, 103, 109, 126, 133) reported an increase with age. However, the two articles with the largest study cohorts (n= 623 and 200) found no change in SVR index (*i.e.* indexed to body surface area) and SVR in men (45, 126). Consequently, it was not clear whether SVR changes with age. Therefore, we calculated peripheral vascular resistance (PVR) values which would result in realistic mean arterial pressure (MAP) values. Changes in MAP with age, and normal variation in MAP, were modelled using male data from (100), the same study used for DBP. Mean values for each age were obtained by interpolating the data using cubic spline interpolation, whilst values for normal variation in MAP were obtained using linear interpolation. The resistance of each vascular bed was adjusted from its baseline value (specified in (108)) to achieve the desired MAP. The total values for each bed were split between each branch feeding into that bed by setting the Windkessel resistances to be inversely proportional to the branch's luminal area (30).

All of the articles identified which investigated changes in systemic vascular compliance (SVC) with age (35, 92, 94, 101, 130) reported a decrease with age. The largest studies estimated large and small artery compliances from brachial and radial pressure PWs (101, 130). These

observed a reduction in both large and small artery compliances with age, indicating that the reduction in SVC with age is not solely caused by changes in larger arteries, but is also contributed to by the rest of the circulation. Therefore, it was assumed that peripheral vascular compliance (PVC) decreased with age. Baseline PVC values corresponding to the 25-year old model were obtained from (108). Changes in PVC with age were modelled using the equation for oscillatory (small artery) compliance provided in (101). Normal variation in PVC was modelled using the results for oscillatory compliance reported in (130).

2.2.4 Blood Properties

Blood density and viscosity were assumed to be constant since there is little evidence to suggest they change with age (80).

2.3 Generating a Database of Arterial Pulse Waves

A preliminary set of PWs was created for the 25-year old subject to determine which cardiovascular properties should be varied in the database. PWs were firstly simulated using the baseline cardiovascular properties, and then by changing each property independently by $\pm$ 1 standard deviation (SD) from its mean value. The resulting PWs at the carotid and radial arteries are shown in Figure 3. Six of the ten properties were found to strongly influence PWs (HR, SV, LVET, diameter, PWV and MAP), whereas the remainder did not (PFT, RFV, proximal aortic length and PVC). Only those properties which strongly influenced PWs were varied at each age to mimic normal physiological variation in the database.

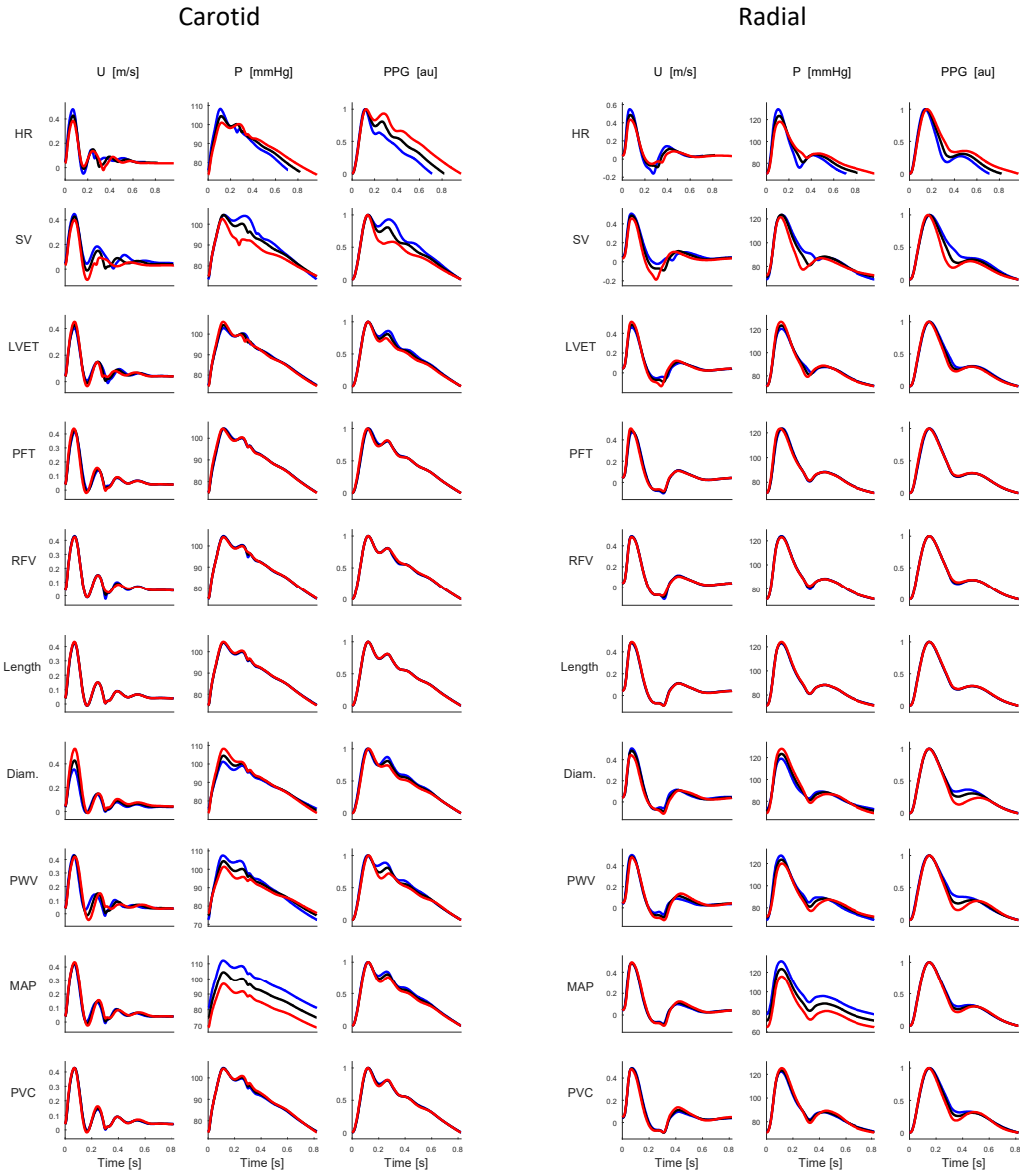

Figure 3: PWs for the 25-year old subject at the carotid artery (left panel) and the radial artery (right panel). The waves shown are at baseline (black), and those obtained when increasing (blue) and decreasing (red) each parameter independently by 1 SD from its baseline value.

304

305 A database of PWs was created by simulating PWs for subjects of each age decade from 25
306 to 75 years. PWs were sampled at 500 Hz. Firstly, PWs were simulated for a baseline subject at each
307 age (using the age-specific mean value for all properties described in Section 2.2). Secondly, PWs
308 were simulated for 3^6 = 729 subjects at each age by changing the six identified cardiovascular

properties in combination with each other by ± 1 SD from their age-specific mean values. This resulted in 6x729 = 4,374 subjects in the database. Thirdly, the plausibility of each subject was investigated by comparing their aortic and brachial BPs (SBP, DBP, MAP, PP and PP_{amp}) to reference healthy values from (100). A subject was deemed to exhibit implausible BPs if any of the BP measurements were outside 99% confidence intervals calculated as the age-specific mean ± 2.575 SD.

2.4 Extracting Pulse Wave Indices

PW indices which are commonly measured in clinical practice or research were extracted from PWs. Firstly, haemodynamic parameters were extracted from flow and pressure PWs at the aortic root. SV, cardiac output (CO), LVET, PFT and RFV were extracted from the flow PW. HR and maximal dP/dt were extracted from the pressure PW. Secondly, systolic (SBP), diastolic (DBP), mean (MAP) and pulse pressure (PP) values were extracted from pressure PWs at common measurement sites. Thirdly, pulse pressure amplification (PP_{amp}) was calculated as the ratio of brachial to aortic PP. Fourthly, pulse transit times (PTTs) were measured along the following paths: carotid-femoral, carotid-radial, femoral-ankle, aortic (*i.e.* aortic root to iliac bifurcation), and between the aortic root and each measurement site. PTTs were measured from pressure waves using the foot-to-foot algorithm reported in (51, 53). PWVs were calculated from the PTTs and corresponding arterial path lengths. Fifthly, indices of arterial stiffness were calculated from the aortic root pressure PW (augmentation pressure and index, and the time to reflected wave) and the digital PPG (modified ageing index, reflection index and stiffness index).

A range of additional PW indices which have been proposed in the literature were also calculated. The timings and amplitudes of the following fiducial points were calculated: P1, P2, systolic peak, and point of maximal dP/dt on the pressure PWs; a, b, c, d, e, systolic peak, diastolic peak, dicrotic notch, and point of maximal dPPG/dt on the PPG PWs. These points were identified

using the *PulseAnalyse* script (described in the Appendix, Section 5.4; see the Endnote for access), which analyses the PWs and their derivatives as shown in Figure 4. P1 and P2 have previously been reported as the first inflection point, and second systolic peak, on the central pressure PW, indicative of the times of maximum aortic flow velocity, and maximum augmentation pressure due to wave reflection, respectively (91). They are used to calculate the augmentation index, as P1 occurs at the arrival of a reflected wave, and P2 occurs as the peak of the reflected wave. In addition, the following values were calculated at the aortic root: the volume of flow up to each of the times of P1 and P2, and the flow velocity at P1 and P2. Finally, the mean, maximum and minimum values of the Q, U and A PWs were extracted.

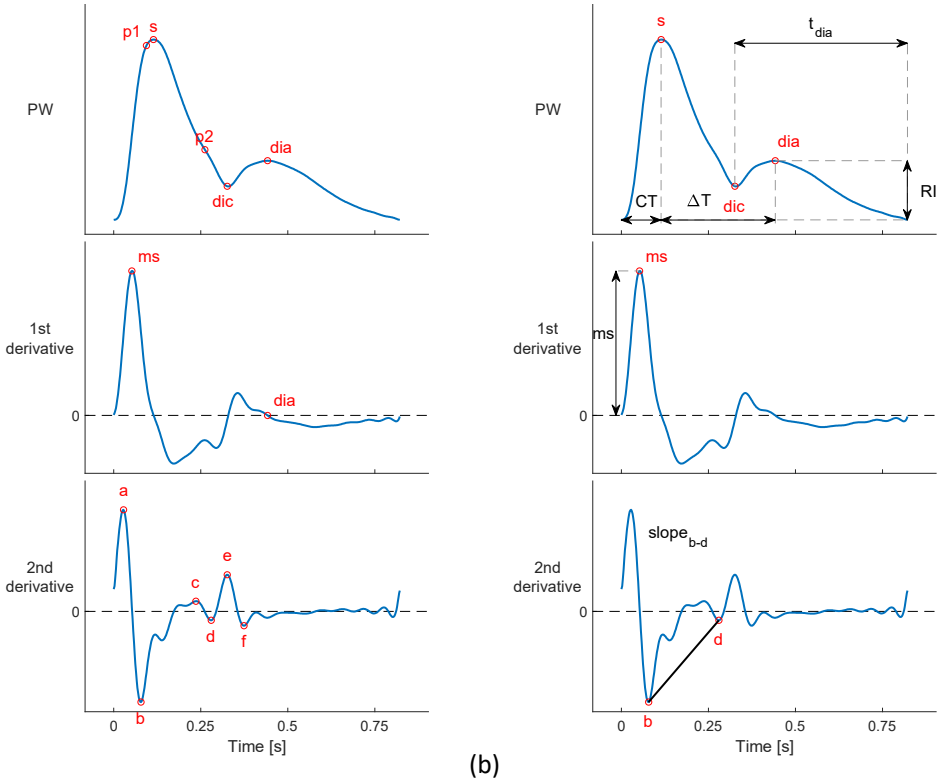

Figure 4: Pulse wave (PW) analysis, illustrated for a radial pressure PW. (a) Fiducial points were identified on the PW, and its first and second derivatives; (b) several pulse wave indices were calculated from the amplitudes and timings of these fiducial points, including those shown.

347 **2.5 Comparison with *In Vivo* Data**

348 The PW database was verified by comparing the simulated PWs with two sets of *in vivo* data
349 from healthy subjects. Firstly, the shapes of simulated PWs for virtual subjects of different ages were
350 compared with *in vivo* PWs at different ages obtained from: (46) [CC BY]; normotensive subjects
351 during screening for hypertension (including aortic root pressure PWs estimated using a transfer
352 function) (90); and, the Vortal dataset (28, 29) [CC BY 3.0]. Additional comparisons of PW shapes
353 were performed using data from (5, 6, 41, 48, 68, 79, 101, 102, 173) (results not shown). Secondly,
354 the haemodynamic characteristics of the simulated PWs were compared to the *in vivo*
355 haemodynamic values reported in (100).

356 **2.6 Case Studies**

357 The utility of this approach for simulating PWs is demonstrated in three case studies. In the
358 first study, we investigated the determinants of changes in pulse pressure amplification (PP_{amp}) with
359 age. To do so, we assessed the effects of age on early systolic amplification and late systolic aortic
360 pressure augmentation, quantified as PP_{amp} calculated using the aortic PP at P1 and P2 respectively.
361 Secondly, we investigated how well the following finger PPG PW indices correlate with aortic PWV:
362 RI, reflection index (38); SI, stiffness index (105); and AGI_{mod}, modified ageing index (159). Reference
363 aortic PWV was calculated from pressure PWs using the foot-to-foot method (53), correlations were
364 assessed using the coefficient of determination (R^2, the square of the Pearson correlation
365 coefficient) and the determinants of the indices were assessed using the relative sensitivity index
366 (which indicates the percentage change in a PW index associated with a change in model input
367 parameter of 1 SD from baseline (170)). In the third study, we assessed how well algorithms for
368 tracking cardiac output (CO) perform during changes in CO and MAP from baseline. Two algorithms
369 were implemented to estimate CO from the radial pressure PW based on the 2-element Windkessel
370 model of the circulation (25). The first algorithm is based on the assumption that CO is proportional
371 to the root-mean-square of the radial pressure PW (25). The second algorithm is based on the

assumption that CO is proportional to the ratio of PP to compliance, approximated as $PP/(T \times (SBP + DBP))$, where T is the PW duration, SBP and DBP are systolic and diastolic BP, and compliance is assumed to be proportional to mean BP (93, 116). These algorithms were chosen as it has been reported that similar algorithms are used in commercial devices (176). The algorithms were calibrated using the age-specific baseline simulations. Performance was assessed using the mean absolute percentage errors (MAPEs) of estimated COs in simulations in which either CO (*i.e.* HR or SV), or MAP were varied whilst all other parameters were held at baseline.

3 Results

3.1 Database Characteristics

The PWs contained within the database are illustrated in Figure 5. There are marked differences between PWs at different sites, such as: the increase in systolic pressure and the transition from an A- to C-type pressure wave shape with distance from the aortic root (109); the genesis of a diastolic peak in flow velocity in the limbs, which is accompanied by diastolic peaks in the other PWs at limb sites; and the genesis of a second systolic peak in flow velocity at the carotid artery, accompanied by second systolic peaks in area and PPG PWs at the temporal artery, which bifurcates from the carotid artery.

A total of 537 out of the 4,374 virtual subjects exhibited BPs outside of healthy ranges. This was predominantly due to abnormal PP (observed in 431 subjects) and abnormally high PP_{amp} (90 of the remainder). Most of the subjects with abnormally high PP had increased PWV, and often had at least one of increased SV, increased MAP, and decreased large artery diameter. The subjects with abnormally low PP had the opposite characteristics: decreased PWV, and at least one of decreased SV, decreased MAP, and increased diameter. Most of the remaining subjects with abnormally high PP_{amp} had decreased PWV, and often increased HR or decreased MAP. The proportion of subjects

396 exhibiting implausible BPs increased with age (from 3% of 25 year olds to 32% of 75 year olds). Only
397 those subjects with BPs within healthy ranges were included in the following analyses.
398

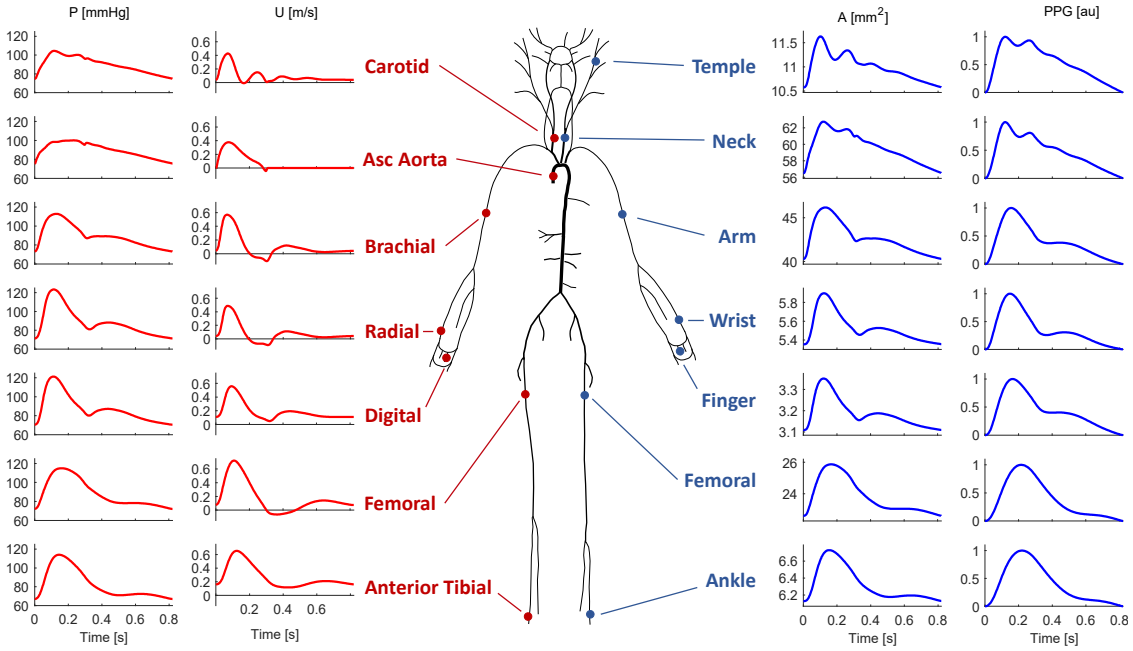

399

400 Figure 5: The pressure (P), flow velocity (U), luminal area (A) and photoplethysmogram (PPG)
401 pulse waves simulated at common measurements sites for the baseline 25-year old subject
402 (adapted from (30) [CC BY 3.0]).

403 The haemodynamic characteristics of the PW database are summarised in Table 1, showing
404 the wide range of cardiovascular physiology exhibited by subjects in the database, both across the
405 whole age range and at each age. Some of the parameters were prescribed to the model and were
406 therefore pre-determined, such as heart rate and proximal aortic length. In contrast, many of the
407 haemodynamic PW parameters were not prescribed directly, but were determined from simulated
408 PWs, such as systolic blood pressure, pulse pressure amplification, and carotid augmentation index.
409 There were marked changes in these resultant parameters with age, indicating that the different
410 values of input parameters prescribed at each age did result in changes in PW shape as seen *in vivo*.

Table 1: The haemodynamic characteristics of the PW database for all physiologically plausible virtual subjects (n = 3,837) and for the subjects at each age, from 25 to 75 years old. Shown as mean ± standard deviation.

Haemodynamic Characteristic	**All Subjects**	**25**	**35**	**45**	**55**	**65**	**75**
Number of physiologically plausible subjects	3,837	712	684	654	641	588	558
Cardiac							
- HR: Heart rate [bpm]	75.6 ± 9.2	73.0 ± 9.1	76.3 ± 9.1	77.0 ± 9.0	77.0 ± 9.1	76.3 ± 9.0	74.4 ± 9.0
- SV: Stroke volume [ml]	60.4 ± 12.4	66.8 ± 13.1	64.1 ± 12.5	61.3 ± 11.6	58.7 ± 11.1	55.8 ± 10.4	53.6 ± 9.8
- CO: Cardiac output [l/min]	4.57 ± 1.09	4.88 ± 1.13	4.90 ± 1.13	4.72 ± 1.06	4.52 ± 1.02	4.25 ± 0.95	3.99 ± 0.86
- LVET: Left ventricular ejection time [ms]	283 ± 23	283 ± 23	284 ± 23	283 ± 23	282 ± 23	282 ± 23	282 ± 23
- dP/dt: Maximum aortic value [mmHg/s]	573 ± 127	585 ± 130	572 ± 132	573 ± 126	570 ± 128	568 ± 119	568 ± 122
- PFT: Peak flow time [ms]	80.0 ± 0.2	79.9 ± 0.4	80.0 ± 0.0	80.0 ± 0.0	80.0 ± 0.0	80.0 ± 0.1	80.0 ± 0.2
- Reverse flow volume [ml]	0.7 ± 0.0	0.7 ± 0.0	0.7 ± 0.0	0.7 ± 0.0	0.7 ± 0.0	0.8 ± 0.1	0.8 ± 0.1
Arterial							
- Aortic pressure [mmHg]: SBP	108.8 ± 10.1	100.1 ± 8.0	104.6 ± 8.4	110.1 ± 8.4	111.9 ± 8.7	113.6 ± 8.7	115.1 ± 9.4
- DBP	75.9 ± 6.7	74.7 ± 5.7	77.3 ± 6.0	78.9 ± 6.1	77.4 ± 6.2	74.8 ± 6.6	71.7 ± 7.2
- MAP	93.9 ± 6.5	89.2 ± 6.2	92.8 ± 6.1	96.3 ± 6.1	96.2 ± 6.0	95.4 ± 5.9	94.2 ± 5.8
- PP	32.9 ± 11.1	25.4 ± 7.0	27.3 ± 8.3	31.3 ± 8.5	34.5 ± 9.4	38.9 ± 10.2	43.4 ± 12.3
- Brachial pressure [mmHg]: SBP	118.1 ± 9.2	112.3 ± 8.7	115.9 ± 9.1	120.4 ± 8.6	120.6 ± 8.5	120.2 ± 8.3	120.1 ± 8.7
- DBP	73.4 ± 6.7	72.0 ± 5.6	74.5 ± 6.1	76.3 ± 6.2	75.0 ± 6.3	72.3 ± 6.6	69.5 ± 7.1
- MAP	93.7 ± 6.6	88.9 ± 6.1	92.5 ± 6.3	96.1 ± 6.1	96.1 ± 6.0	95.2 ± 5.9	94.0 ± 5.8
- PP	44.7 ± 10.2	40.3 ± 8.2	41.5 ± 9.2	44.1 ± 9.1	45.6 ± 9.6	47.9 ± 9.8	50.6 ± 11.5
- Pulse pressure amplification (ratio)	1.41 ± 0.21	1.62 ± 0.15	1.56 ± 0.16	1.44 ± 0.13	1.35 ± 0.13	1.26 ± 0.11	1.19 ± 0.10
- Augmentation pressure (carotid) [mmHg]	8.0 ± 8.2	0.6 ± 3.0	2.5 ± 3.6	5.9 ± 4.4	9.4 ± 5.2	13.9 ± 6.4	18.8 ± 8.4
- Augmentation index (carotid) [%]	20.6 ± 16.8	2.3 ± 10.4	8.4 ± 10.7	17.8 ± 10.2	25.9 ± 9.4	34.3 ± 8.9	41.5 ± 9.1
- Time to reflected wave (carotid) [ms]	102.3 ± 19.3	122.4 ± 9.1	115.6 ± 11.7	104.7 ± 13.0	96.2 ± 13.9	87.2 ± 12.9	80.2 ± 13.2
- Pulse wave velocity [m/s]: aortic	7.6 ± 1.7	5.9 ± 0.6	6.5 ± 0.8	7.3 ± 0.9	8.0 ± 1.1	8.9 ± 1.3	9.7 ± 1.6
- carotid-femoral	8.1 ± 1.8	6.3 ± 0.7	6.9 ± 0.9	7.8 ± 0.9	8.5 ± 1.1	9.5 ± 1.4	10.4 ± 1.9
- brachial-radial	10.7 ± 1.7	8.9 ± 0.6	9.5 ± 0.8	10.4 ± 0.8	11.1 ± 1.0	12.0 ± 1.3	12.8 ± 1.6
- femoral-ankle	10.3 ± 1.7	8.7 ± 0.9	9.2 ± 1.1	10.1 ± 0.8	10.7 ± 1.0	11.6 ± 1.2	12.4 ± 1.5
- Diameter [mm]: ascending aorta	39.4 ± 3.5	36.7 ± 2.6	37.8 ± 2.7	39.0 ± 2.8	40.2 ± 2.9	41.4 ± 3.0	42.6 ± 3.0
- descending thoracic aorta	26.3 ± 2.3	24.4 ± 1.7	25.2 ± 1.8	26.0 ± 1.9	26.8 ± 1.9	27.6 ± 2.0	28.3 ± 2.0
- abdominal aorta	15.6 ± 1.3	14.5 ± 1.0	15.0 ± 1.1	15.4 ± 1.1	15.9 ± 1.1	16.3 ± 1.2	16.8 ± 1.2
- Length of proximal aorta [mm]	95.1 ± 10.9	80.0 ± 0.0	86.4 ± 0.0	92.8 ± 0.0	99.2 ± 0.0	105.6 ± 0.0	112.0 ± 0.0
- Modified Ageing Index [au]	-0.78 ± 0.46	-0.98 ± 0.24	-1.00 ± 0.25	-0.89 ± 0.33	-0.76 ± 0.43	-0.56 ± 0.52	-0.41 ± 0.59
- Reflection Index [au]	0.28 ± 0.14	0.18 ± 0.08	0.21 ± 0.10	0.27 ± 0.11	0.31 ± 0.11	0.36 ± 0.12	0.41 ± 0.13
- Stiffness Index [m/s]	7.8 ± 2.4	6.2 ± 1.0	6.7 ± 1.1	7.5 ± 1.0	8.1 ± 1.6	8.9 ± 2.8	10.3 ± 3.4
Vascular Beds							
- Systemic vascular resistance [10^6 Pa s/m^3]	173.7 ± 42.5	153.8 ± 34.5	159.5 ± 36.5	171.2 ± 38.3	178.9 ± 41.0	188.6 ± 43.8	198.1 ± 45.1
- Peripheral vascular compliance [10^9 m^3/Pa]	29.3 ± 7.7	40.1 ± 0.0	35.5 ± 0.0	31.0 ± 0.0	26.4 ± 0.0	21.9 ± 0.0	17.3 ± 0.0
- Time constant [s]	1.07 ± 0.39	1.30 ± 0.41	1.22 ± 0.42	1.12 ± 0.36	1.02 ± 0.32	0.90 ± 0.28	0.82 ± 0.26

411

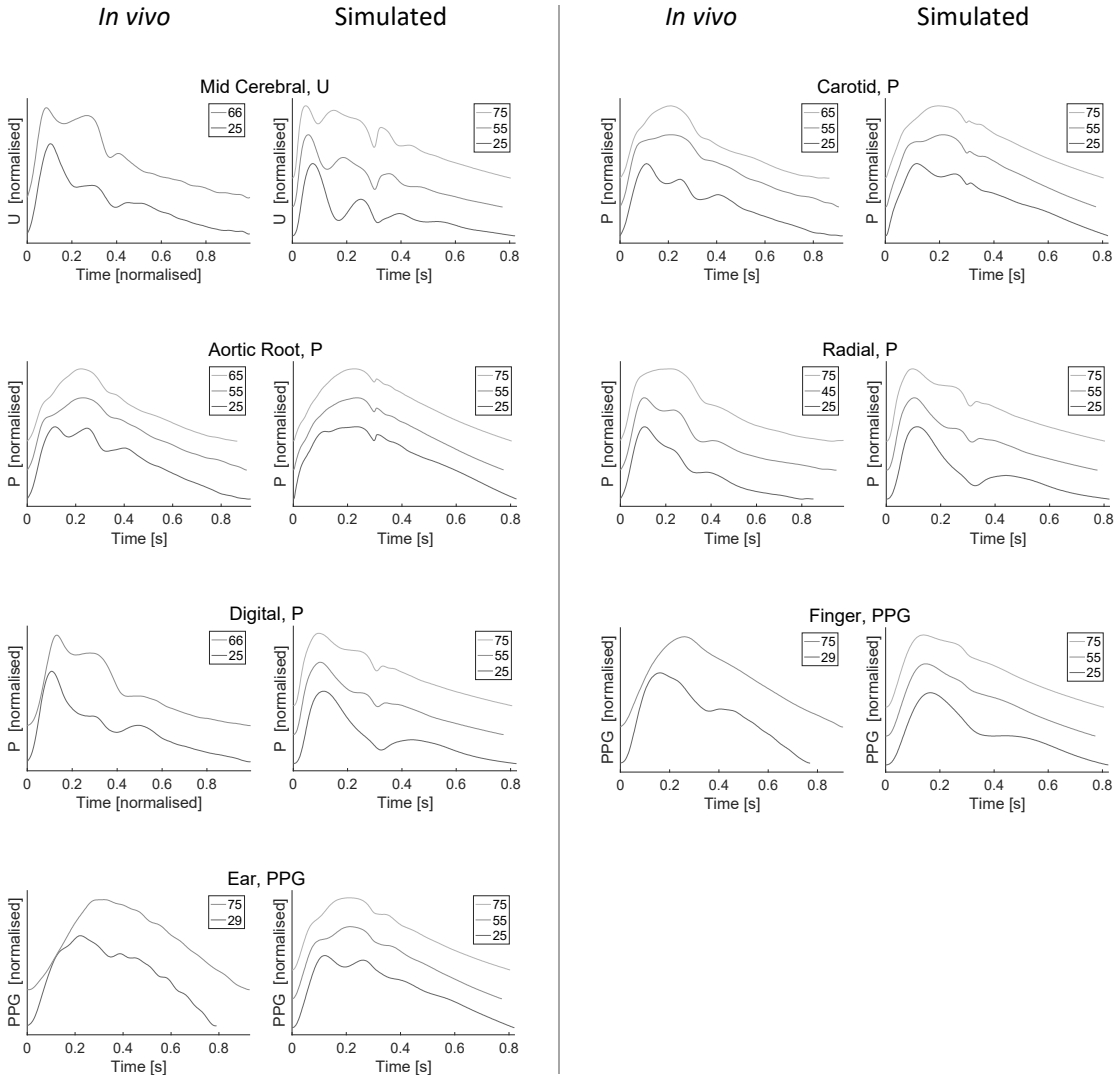

Figure 6: A comparison between simulated and *in vivo* pulse wave (PW) shapes. Each pair of plots shows *in vivo* PWs on the left, and simulated PWs on the right. PWs are shown for different ages in each plot, offset and normalised. Legends indicate ages. *In vivo* data obtained from (46) [CC BY], normotensive patients undergoing screening for hypertension (90), and the Vortal dataset (28, 29) [CC BY 3.0].

3.2 Comparison with *In Vivo* Data

A selection of the simulated PWs are compared to PWs from the literature in Figure 6. PWs from both the PW database (simulated) and the literature (*in vivo*) are shown for young, middle-aged, and elderly subjects. The shapes of the simulated PWs changed with age in a similar manner to

the *in vivo* PWs: (i) the amplitude of the secondary systolic peak in middle cerebral U PWs increased with age; (ii) the augmentation in the secondary systolic peak of the carotid and ascending aorta pressure PWs increased with age; (iii) the diastolic peak in the radial, digital and femoral (not shown) pressure PWs was present for the 25-year old and disappeared with age; (iv) the diastolic peak of the finger PPG PW disappeared with age; (v) the two systolic peaks in the ear PPG merged with age.

The haemodynamic characteristics of the simulated PWs are compared with those in the literature in Figure 7. The changes with age were mostly similar between the literature (left hand plots) and simulated (right hand plots) characteristics: aortic systolic and pulse pressures increased with age; pulse pressure amplification (PP_{amp}) decreased with age; the time to the return of the reflected pressure wave (Tr) decreased with age; and pressure augmentation increased with age (AIx and AP). However, brachial PP increased with age, rather than decreasing and then increasing with age. This was because the brachial SBP was slightly lower than in the literature at ages 25 and 35. Overall, these similarities indicate that the haemodynamic characteristics of the simulated PWs showed similar trends, and in most cases similar absolute values, to those reported in the literature.

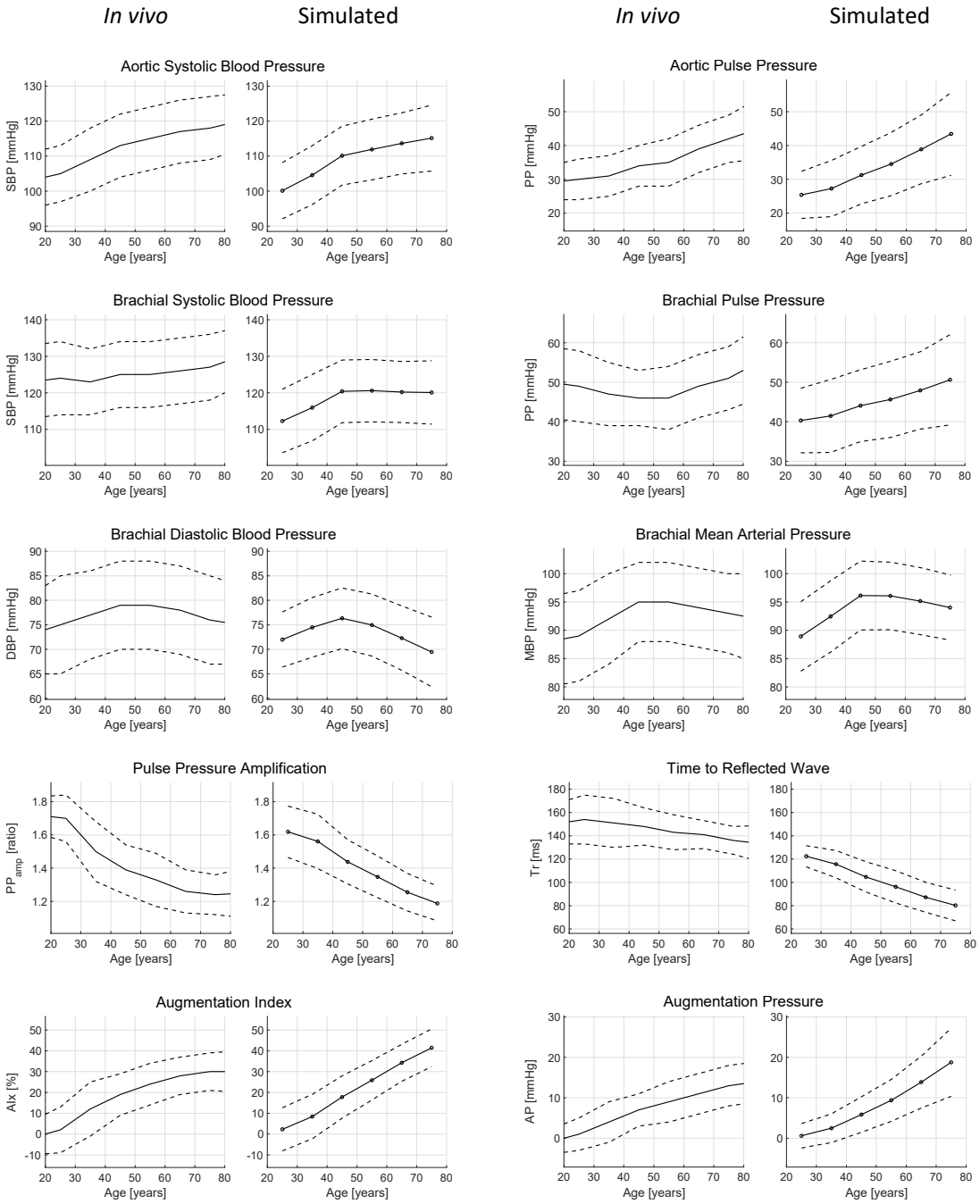

Figure 7: A comparison between *in vivo* haemodynamic characteristics (left hand plots) and the characteristics of the simulated pulse wave dataset (right hand plots). Solid lines indicate mean values, and dashed lines indicate ± 1 standard deviation. *In vivo* data from source (100), reused with confirmation from the publisher that permission was not required for reuse.

437

3.3 Case Studies

3.3.1 The Determinants of Changes in Pulse Pressure Amplification with Age

The profiles of pressure PW propagation from the aorta to the brachial artery were examined in young and elderly subjects, as shown in Figure 8 (a) and (b). The profiles demonstrate that two mechanisms influence pulse pressure amplification ($PP_{amp} = PP_b / PP_a$; subscripts 'a' and 'b' indicate aortic and brachial, respectively). Firstly, the early systolic portion was amplified in both subjects, causing SBP_b to be greater than SBP_a and therefore $PP_{amp} > 1$. Secondly, late systolic aortic pressure augmentation (the increase in pressure from $P1_a$ to $P2_a$) was higher in older subjects, increasing PP_a and decreasing PP_{amp}. The contributions of these mechanisms to PP_{amp} for the whole database are illustrated in Figure 8 (c). The amplification of the early systolic portion increased with age, as shown in red by $PP_b / (P1_a – DBP_a)$. In contrast, the increase in late systolic aortic pressure augmentation with age (in blue) caused a decrease in $PP_b / (P2_a – DBP_a)$ with age. The effect of aortic pressure augmentation outweighed that of early systolic amplification, meaning PP_{amp} decreased substantially with age, in keeping with *in vivo* studies (Figure 7). The database can be used to gain insight into the cardiovascular determinants of these mechanisms: early systolic amplification was determined primarily by the diameter of the larger arteries, and late systolic aortic pressure augmentation was largely determined by PWV and LVET, as shown in Figure 8 (d) and (e). Indeed, since PP_{amp} was primarily determined by late systolic aortic pressure augmentation, it was largely determined by arterial stiffness (*i.e.* PWV) and LVET, as shown in Figure 8 (f). The change in PP_{amp} observed with age was primarily due to changes in aortic pressure wave morphology.

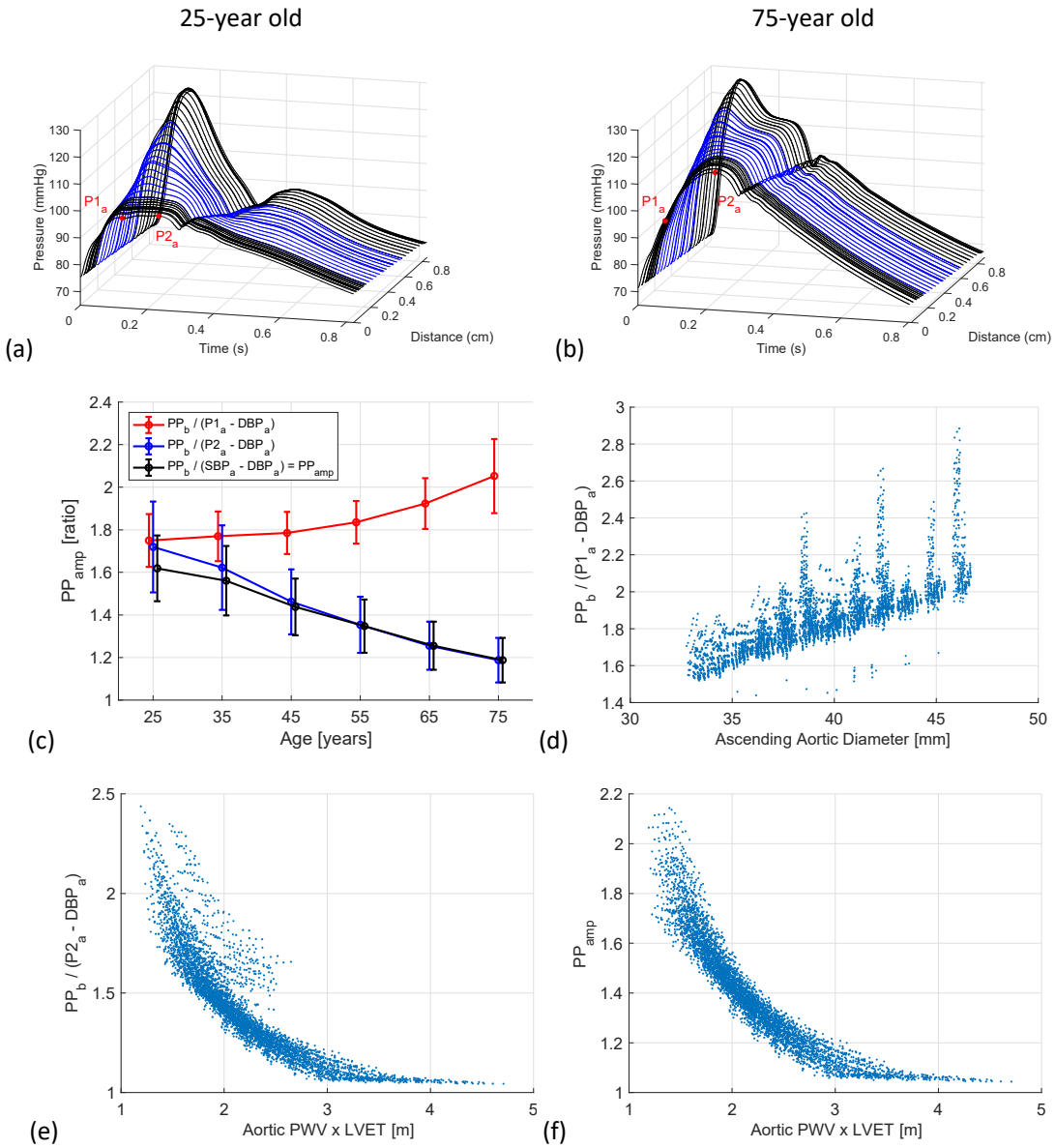

Figure 8: The causes of changes in pulse pressure amplification (PP_{amp}) with age: (a) and (b) show how the pressure pulse wave (PW) changed with distance along the path from the aortic root to the finger for young and elderly baseline subjects (blue indicates PWs in the subclavian and brachial arteries). (c) shows PP_{amp} values (mean ± SD) calculated using aortic DBP and: SBP (black), early systolic pressure ($P1_a$, red) and late systolic pressure ($P2_a$, blue). (d) , (e) and (f) show the principal cardiovascular determinants of early systolic amplification, late systolic augmentation and PP_{amp} respectively

458

3.3.2 Non-Invasive Peripheral Assessment of Aortic Stiffness

The performance of the PPG-derived indices for assessing aortic stiffness is shown in Figure 9. All three correlated with aortic PWV, with similar coefficient of determination (R^2) values ranging from 0.66 – 0.70 (upper plots). This indicates that these indices may have utility for assessing aortic stiffness, in line with findings of clinical studies. However, the R^2 values for the reflection index (RI) and stiffness index (SI) were lower when using only data from middle-aged (45 year old) virtual subjects (shown in red), indicating that these indices may be less useful for stratifying middle-aged patients. The sensitivity analyses in the lower plots quantify the relative impact of different input parameters on the indices. Several cardiovascular properties in addition to PWV influenced the indices, such as HR and SV. For instance, the RI and SI both increased with large artery diameter. Since large artery diameter and aortic PWV both increase with age, this strengthened their correlations with aortic PWV across the age range. In contrast, the AGI_{mod} was not strongly influenced by large artery diameter, and performed better both across the age range and when considering only middle-aged subjects. This *in silico* assessment of PPG-derived indices for assessing aortic stiffness indicates that: (i) clinical studies should investigate performance over a small age range as well as over the entire cohort to assess the potential utility of indices for stratifying patients; (ii) the AGI_{mod} may provide best performance for stratification of middle-aged patients; (iii) indices can also be influenced by HR and SV, indicating that it may be beneficial to assess performance when these cardiovascular properties are varied *in vivo*.

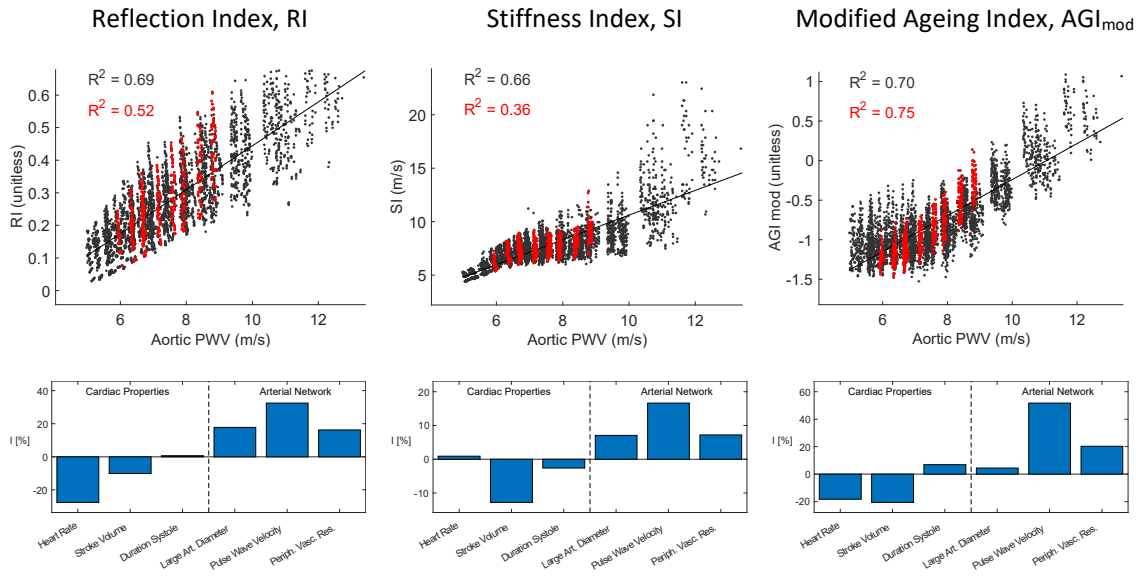

Figure 9: The correlation of PPG-derived PW indices with aortic PWV (upper plots), and their physiological determinants (lower plots). Data derived for all virtual subjects are shown in black, whereas red indicates data from 45 year old subjects. Definitions: I, relative sensitivity index; RI, reflection index; SI, stiffness index; and AGI$_{mod}$, modified ageing index.

3.3.3 Cardiac Output Monitoring

The performance of the CO algorithms is shown in Figure 10. Overall, the root-mean square (RMS) algorithm performed better with a mean absolute percentage error (MAPE) of 5.5% compared to 18.2% for the pulse pressure (PP) algorithm. However, a subgroup analysis of performance during changes in MAP and CO revealed that the algorithms had different strengths and weaknesses. The PP algorithm performed better during changes in MAP (MAPE of 2.2% compared to 7.9%), whereas the RMS algorithm performed better during changes in CO (MAPE of 1.0% compared to 16.2%). Therefore, different algorithms may be more appropriate for different clinical settings. For instance, in the critical care setting CO algorithms should ideally remain accurate during administration of vasoactive drugs, which can affect MAP (105). Furthermore, clinical studies should assess the performance of CO algorithms during changes in those cardiovascular properties

497 which would be expected to change in clinical use. Had this study only considered changes in CO,
498 and not MAP, then the potential weakness of the RMS algorithm would not have been identified.
499

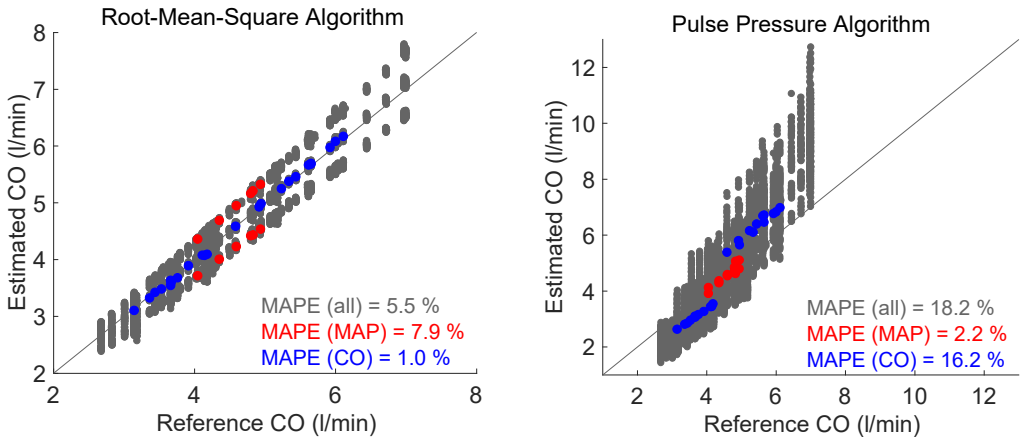

500

501 Figure 10: Estimated versus reference cardiac output (CO) for root-mean-square (left) and pulse
502 pressure (right) CO algorithms. Data in red and blue correspond to simulations in which either
503 MAP or CO respectively were changed from baseline whilst all other parameters were held
504 constant.

505
506
507
508
509
510
511
512
513
514
515

4 Discussion

In this study we developed and verified an approach for simulating PWs representative of a sample of healthy adults. 1D numerical modelling was used to simulate PWs for virtual subjects of different ages, where the input parameters were based on normal values and ranges of cardiovascular properties obtained from a comprehensive review of previous studies. The simulated PWs exhibited similar changes with age to those reported in *in vivo* studies, including changes in PW shape and in haemodynamic parameters derived from PWs. The utility of this approach for gaining novel insights into haemodynamics and PW indices was demonstrated through three case studies. The approach for simulating PWs, the resulting PW Database, and the accompanying code are valuable resources for future *in silico* studies of haemodynamics and PW indices.

4.1 Approach for Simulating PWs

We used 1D modelling combined with a comprehensive review of cardiovascular changes with age to simulate PWs around the body for healthy subjects of different ages. The use of 1D modelling allowed us to simulate PWs at a range of common measurement sites similarly to previous studies (108, 170), incorporating the effects on PW propagation of changing arterial properties through the arterial tree. The model input parameters were adjusted to simulate PWs for different ages. The input parameters were based on a literature review which identified normal values and ranges of the parameters, building on previous reviews (17, 47, 78, 84–86, 99, 110, 113, 135). Parameters were changed with age, allowing the effects of ageing to be investigated, and were also varied within normal ranges at each age, allowing the influences of individual parameters to be elucidated. This builds on previous work modelling changes with age in (34, 39, 59, 60, 95, 115, 120).

Particular strengths to this approach are as follows. Firstly, it incorporates relationships between some input parameters, including the dependencies of: LVET on SV and HR; and arterial stiffness on MAP and arterial geometry. Secondly, it simulates the PPG, which is of particular interest

given the widespread use of PPG sensors in smart watches and fitness bands. We simulated the PPG from the blood volume in terminal Windkessel models because pulsatile blood volume is commonly cited as the main determinant of the PPG (4). Other approaches which have previously been used to simulate the PPG in 1D modelling include: assuming the PPG is proportional to A (44), and using a transfer function to estimate the PPG from P (30). This methodology for simulating the PPG needs further investigation to understand whether it is truly representative of PPG PWs measured *in vivo*.

The approach was verified by comparing changes in simulated PWs with age to those observed *in vivo*. The main finding, that simulated PWs exhibited similar changes to those observed *in vivo*, provides confidence that the approach produces realistic changes with age. This is complementary to previous studies which used 1D modelling to simulate PWs at different ages (59, 61, 115).

The main limitations to the approach are as follows. Firstly, the literature review included mostly cross-sectional rather than longitudinal studies. Consequently, the differences in simulated PWs with age can be expected to be representative of those which would be observed between subjects of different ages, rather than those which occur within an individual over time. Secondly, we found only minimal evidence in the literature describing how some CV properties change with age, namely: PVC and the diameters of more peripheral arteries. Thirdly, insufficient evidence was found to model the associations between certain parameters. For instance, the subjects with abnormally high PP (described in Section 3.1) mostly had combinations of cardiovascular properties which would be expected to produce high PP; *e.g.* due to increased SV and/or decreased arterial compliance (35). It would be helpful to incorporate further information on correlations between parameters, such as those which influence PP, when it becomes available in the literature: doing so may reduce the number of subjects exhibiting BPs outside healthy ranges. Fourthly, the approach does not incorporate methodology for adjusting the arterial network geometry in line with variation in height and body surface area, an important consideration when investigating gender-associated

565 differences in haemodynamics (134). This may be a valuable extension in the future as it would allow
566 for investigation of the influence of network geometry on haemodynamics, such as the influence of
567 height on aortic pressure augmentation (11, 71, 72) and pulse pressure (88). Indeed, incorporating
568 gender-specific cardiovascular properties could provide valuable insight into the determinants of
569 differences in PW features between females and males (100). Fifthly, the PW database is designed to
570 be representative of healthy adults: it may be helpful to adapt it to study PWs in diseases such as
571 hypertension and peripheral arterial disease. It should also be noted that PPG PWs can only be
572 measured at peripheral locations (such as the finger, wrist and arm). Consequently, simulated PPG
573 PWs at central locations (such as the aorta) are currently not of practical significance.

574 **4.2 Application**

575 The utility of the approach for simulating PWs was demonstrated through case studies
576 which present interesting findings in keeping with *in vivo* studies, and indicate directions for future
577 research.

578 The first case study provided insight into the mechanisms underlying changes in PP_{amp} with
579 age. PP_{amp} has previously been proposed as an indicator of cardiovascular risk suitable for use in
580 population studies (14). If it is to be used for this purpose then it is important to have a thorough
581 understanding of the mechanisms behind it. The first mechanism identified in this study, the
582 increased contribution of late systolic aortic pressure augmentation with age, has also been
583 observed in *in vivo* studies (8, 123, 144, 169). In this case study, the controlled changes in
584 cardiovascular properties in the database were used to identify the determinants of late systolic
585 aortic pressure augmentation: arterial stiffness and cardiac ejection properties, as observed
586 previously (52, 161). The second mechanism, the contribution of early systolic pressure
587 amplification, has been less well reported. A non-significant trend of increased early systolic
588 pressure amplification with age was reported in (167). This case study adds evidence to support this

589 finding, and indicates that this mechanism may be more pronounced in subjects aged 75 years and
590 older.

591 The second and third case studies investigated the performance of PW indices for assessing
592 aortic stiffness and CO. This approach of assessing PW indices *in silico* could inform the design of
593 future clinical studies. In both case studies the PW indices were found to be influenced by other
594 cardiovascular properties besides those they aimed to assess. PPG-derived indices for assessing
595 aortic stiffness were determined in part by cardiac properties (SV and HR), whilst the accuracy of BP-
596 derived indices for tracking changes in CO was influenced by MAP and CO itself. These findings
597 indicate that future studies of these indices should assess their performance during changes in these
598 properties. In addition, the performance of some indices for assessing aortic stiffness was reduced
599 when only considering subjects of a certain age. Whilst previous *in vivo* studies have provided
600 valuable results across a wide age range (105, 164), this study highlights the importance of also
601 assessing indices across a small age range in order to assess their utility for risk stratification.

602 **4.3 Perspectives**

603 The approach presented for simulating PWs may be useful for obtaining insight into the
604 haemodynamic mechanisms underlying findings of previous *in vivo* studies, and for designing novel
605 *in vivo* studies. Similar approaches have previously been used to identify the mechanisms underlying
606 *in vivo* observations, including: (i) the reasons for differences in the performance of different PWV
607 measurement paths for assessing aortic PWV (170); (ii) the cardiovascular properties which
608 influence a transfer function relating peripheral to central pressure (75, 151); and, (iii) the strengths
609 and weaknesses of physiological measurement devices (116, 157). More recently, studies have used
610 both *in vivo* PW measurements and simulated PWs to obtain novel insights into haemodynamics,
611 including: (i) the determinants of central pulse pressure (161); and (ii) the influence of cardiovascular
612 properties on forward and backward pressure waveform morphology (90). We expect that the

613 approach presented here, which has been verified against *in vivo* data, will be of value for future
614 studies.

615 In the future this approach may form a basis for creating haemodynamic digital twins –
616 simulations of an individual's haemodynamics using input parameters obtained from their
617 physiological measurements (156). This would allow changes in cardiovascular health to be
618 identified when an individual's PWs, acquired by smart wearables, diverge from their digital twin's
619 'normal' PWs, prompting clinical assessment.

620 This article is accompanied by resources to enable other researchers to use this approach for
621 simulating PWs. Firstly, the PW database is freely available to download (32). Secondly, key fiducial
622 points on PWs (such as those labelled in Figure 4) are provided, allowing researchers to use the
623 results of PW analysis without performing any signal processing. Thirdly, the code used to create and
624 analyse the pulse wave database, and for reproducing the case studies is available, allowing
625 researchers to run example analyses and gain an understanding of how to use the database (33).
626 Fourthly, the signal processing tool used to extract PW indices, *PulseAnalyse*, is available (26): it is
627 currently designed for use with this database, and work is ongoing to develop it on independent
628 datasets. Further details of these resources are provided in the Endnote at the end of this article.

629 **4.4 Conclusion**

630 We have designed and verified an approach for simulating PWs representative of healthy
631 adults of different ages. A computational model of the arterial system was used to simulate several
632 types of PWs at common measurement sites for 4,374 virtual subjects. Simulations were performed
633 for subjects of different ages by adjusting model input parameters in line with typical cardiovascular
634 parameters for each age obtained from a comprehensive literature review. The resulting database of
635 PWs exhibited similar age-related changes in haemodynamic parameters and PW morphology to
636 those in previous *in vivo* studies. We demonstrated the utility of the approach through case studies,
637 which provided novel insights into the haemodynamic determinants of PWs and provided pilot data

638 to inform clinical studies of PW algorithms. The database is freely available and is a valuable
639 resource for future research.

640

641

5 Appendix

5.1 Numerical model

5.1.1 Arterial Network Geometry

The geometry of the baseline 25-year old model is provided in the supplementary file called *116_artery_model.txt* . The following information is provided for each of the 116 arterial segments in the baseline model: length, inlet and outlet radii, and inlet and outlet nodes. The geometry for each of the virtual subjects is provided in the Pulse Wave Database.

The geometry was adapted from the arterial network presented in (108), by taking the following steps (which are documented in the supplementary file):

- Segments 1, 2 and 3 in (108), which represent the left ventricular outflow tract, aortic root and ascending aorta, were combined into a single segment (segment 1 in the new network).
- Segments 10, 12 and 14 in (108), which represent the latter part of the right subclavian artery, the right axillary artery, and the right brachial artery, were combined into a single segment (segment 7 in the new network).
- An additional segment (segment 30 in the new network) was added, extending the celiac artery by 10 mm.
- Segments 81, 84, 85, 86, 91, 92, 102, 121 and 123 in (108), representing the basilar artery, the initial parts of the posterior cerebral arteries, the distal internal carotid arteries, and anterior communicating artery, were adjusted (mainly by adjusting their lengths).
- The luminal areas of each segment obtained from (108) were increased by a scaling factor of 1.5 to increase the compliance of the network, and reduce the simulated PPs, making them more similar to those reported in (108).

- We added arterial segments 97-116 in our network to represent the larger arteries of the hand. These were adapted from (3) using the *calculate_hand_artery_segment_radii.m* script (see accompanying code). Briefly, the areas of the distal segments at the junctions at the end of the radial and ulnar arteries were adjusted to achieve area ratios of 1.15 as suggested for matched conditions in (58). The remaining luminal areas of the hand were adjusted from their original values, in line with the adjustments made to achieve matched junctions.

5.1.2 Simulating the PPG

The methodology used to simulate PPG PWs was introduced in Section 2.1. We now provide additional details of the methodology used in the two possible scenarios: (i) at the periphery (*i.e.* the end of a 1D model terminal branch); and (ii) within the arterial network. At the periphery (such as the digital artery in the finger) the PPG was calculated using

$$PPG(t) = \int_0^t Q_{1D}(t') - Q_{out}(t')\, dt' , \quad (5)$$

where Q_{1D} is the inflow to the terminal Windkessel, and Q_{out} is the outflow (as shown in Figure 1). At distal sites within the arterial network (such as the wrist), the PPG was calculated by assuming that the volume of blood in the microvasculature at that site could be modelled by a Windkessel model. The basis for this assumption is that vascular beds at sites within the arterial network are perfused by arterioles branching from the major artery at that site (*e.g.* the radial artery at the wrist) which are too small to be represented in the arterial network. Therefore, the inflow to the Windkessel was assumed to be proportional to the flow through the arterial segment, at a pressure equal to that of the arterial segment. The same equation was used to calculate the PPG, where Q_{1D} was set equal to the flow through the arterial segment, and Q_{out} was calculated using

$$Q_{out}(t) = \frac{P(t) - P_{out}}{R} , \quad (6)$$

where

690 $$R = \frac{\overline{P(t)} - P_{out}}{\overline{Q_{1D}(t)}} \ , \qquad (7)$$

691 and P_{out} is the outflow pressure (with P and Q_{1D} obtained at the point of measurement). This
692 approach was verified by checking that a PPG PW calculated using this approach at the periphery is
693 very similar to the one calculated using the flow in and out of the terminal Windkessel. Figure A11

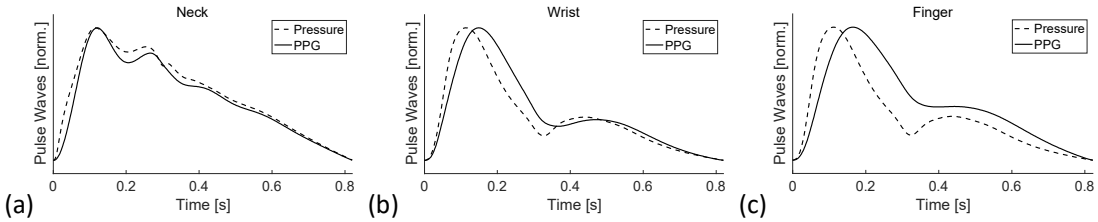

Figure A11: Exemplary simulated PPG pulse waves (solid lines) compared to the corresponding pressure pulse waves at three sites: (a) carotid artery (neck); (b) radial artery (wrist); (c) digital artery (finger). Pulse waves have been normalised to occupy the same range. Taken from the 25-year old baseline subject.

694 shows examples of the resulting PPG PWs at common measurement sites.

695

696 **5.2 Literature review**

697 Table A1 presents the results of the literature review for each model input parameter. Table
698 A2 provides equations for each input parameter and its standard deviation, which were calculated
699 using data from articles selected from the literature review presented in Section 2.2.

Table A1: A summary of the literature review of changes in cardiovascular properties with age. The type of change with age used for each parameter is underlined, and references to the relevant articles are provided in the last columns.

Cardiovascular property	No. studies	No. articles	Change with age (%)				Data Source	
			None	Increase	Decrease	Non-linear	Change	Variation
Cardiac								
- Heart Rate	22	22	86.4	4.5	4.5	4.5	(174)	(119)
- Stroke Volume	11	11	18.2	9.1	72.7	0.0	(121)	(121)
- Left Ventric. Ejection Time	10	10	80.0	10.0	0.0	10.0	(108)	(55)
- Peak Flow Time	3	3	66.7	0.0	33.3	0.0	(74)	(74)
- Reverse Flow Volume	1	1	100.0	0.0	0.0	0.0	(15)	(15)
Arterial								
- Length: proximal aorta	5	4	0.0	100.0	0.0	0.0	(67)	(15)
distal aorta	5	4	60.0	20.0	0.0	20.0	-	-
carotid	1	1	100.0	0.0	0.0	0.0	-	-
iliac	1	1	100.0	0.0	0.0	0.0	-	-
- Diameter: ascending aorta	13	13	7.7	92.3	0.0	0.0	(67)	(1)
descending thoracic aorta	5	5	0.0	100.0	0.0	0.0	(67)	(1)
abdominal aorta	6	6	0.0	100.0	0.0	0.0	(67)	(1)
carotid	6	6	33.3	66.7	0.0	0.0	(63)	(63)
iliac	2	2	50.0	50.0	0.0	0.0	-	-
femoral	3	3	66.7	33.3	0.0	0.0	-	-
brachial	2	2	0.0	100.0	0.0	0.0	-	-
radial	1	1	0.0	100.0	0.0	0.0	-	-
- Pulse wave velocity: aorta	24	19	4.2	95.8	0.0	0.0	(98)	(98)
upper limb	11	11	0.0	100.0	0.0	0.0	(9)	-
lower limb	5	5	20.0	80.0	0.0	0.0	(9)	-
Vascular Beds								
- Systemic vasc. resistance	9	9	44.4	55.6	0.0	0.0	(100)	(100)
- Systemic vasc. compliance	5	5	0.0	0.0	100.0	0.0	(101)	(130)

Table A2: The model input parameters, where the mean and standard deviation can vary with age (in units of years). Coefficients are given to three significant figures. '% of 25-year old' indicates the percentage change from the value(s) in the 25-year old baseline model.

Cardiovascular Property	Mean value	Standard Deviation
Cardiac		
- HR: Heart Rate [bpm]	nonlinear, see text	11.2
- SV: Stroke Volume [ml]	72.7 – 0.253 x age	18.1 – 0.081 x age
- LVET: Left Ventricular Ejection Time [ms]	282	23.3
- PFT: Peak Flow Time [ms]	79.0	11.0
- RFV: Reverse Flow Volume [ml]	0.730	0.630
Arterial		
- Len: Length of proximal aorta [% of 25-year old]	80.0 + 0.800 x age	10.7 + 0.107 x age
- Dia: Diameter of larger arteries [% of 25-year old]	90.9 + 0.365 x age	8.18 + 0.033 x age
- PWV: Pulse wave velocity	nonlinear, see text	nonlinear, see text
Vascular Beds		
- MAP: Mean arterial blood pressure [mmHg]	nonlinear, see text	7.98 – 0.00952 x age
- PVC: Peripheral vascular compliance [% of 25-year old]	128.4 – 1.136 x age	35.2 – 0.311 x age

5.3 Prescribing Model Parameters

5.3.1 The Aortic Inflow Waveform

Each virtual subject's aortic inflow waveform was calculated from the template waveform in order to achieve the desired inflow characteristics (HR, SV, LVET, PFT and RFV). This was performed using the *AorticFlowWave* script (see the Endnote for access), which ensures that the morphology of each segment of the inflow wave (systolic upslope, systolic downslope, and reverse flow) remains the same during changes in inflow wave characteristics. Figure A12 shows the simulated aortic flow waves obtained for independent changes in inflow characteristics from the 25-year old baseline subject, and obtained for baseline subjects of different ages. Note that the values for LVET change when varying HR and SV, in accordance with the relationship between LVET and HR and SV given by Eq. (1). These changes in LVET solely affect the diastolic downslope portion of the flow wave, ensuring that PFT remains constant during these changes.

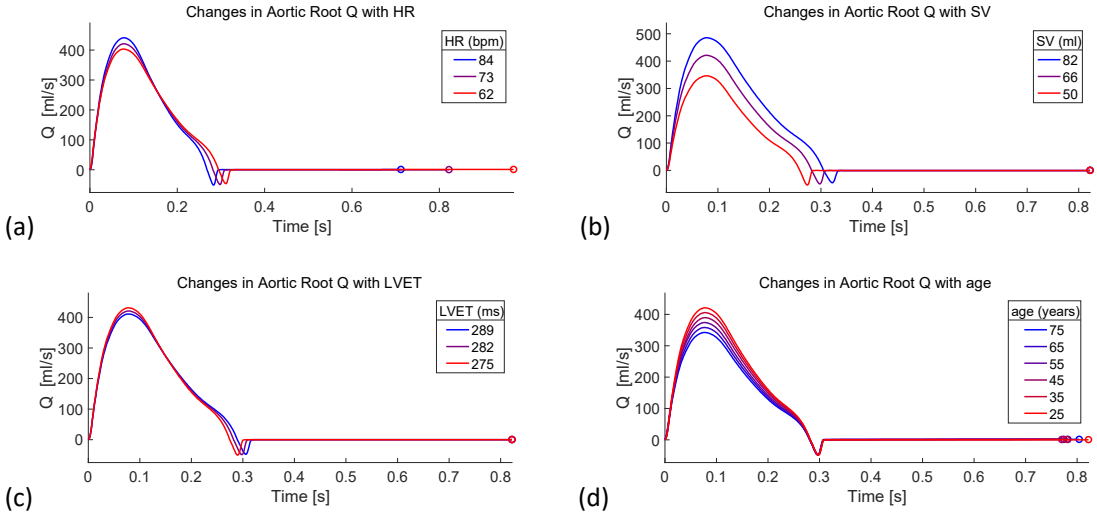

Figure A12: Simulated aortic flow waves obtained for independent changes in inflow characteristics from the 25-year old baseline subject, and obtained for baseline subjects of different ages. (a)-(c) show flow waves obtained by varying HR, SV and LVET by $\pm$ 1 SD from the mean value for the 25-year old baseline subject whilst all other input parameters are held at baseline values. (d) shows flow waves obtained for the baseline subjects of different ages.

720

721

722 **5.3.2 Arterial Stiffness**

723 The relationship between arterial stiffness and radius given by Eq. (2) was adjusted for each
724 virtual subject to minimise the differences between the desired PWVs and the expected PWVs along
725 three paths: carotid-femoral, brachial-radial, and femoral-ankle. This was performed using the
726 *calculate_pwdb_input_parameters.m* script (see the Endnote for access). The values for the
727 constants (k_1, k_2, and k_3) in equation (2) were obtained as follows. k_1, which determines the stiffness
728 of smaller arteries, was set to $3\text{x}10^6$ $gs^{-2}cm^{-1}$ following (108). The value for k_2, which determines the
729 point of transition in stiffness between larger and smaller arteries, was adjusted slightly from the
730 value of -9 cm^{-1} used in (108) to -13.5 cm^{-1}, as this was found to give more realistic PW shapes and
731 pulse pressure amplification. The value for k_3, which determines the stiffness of larger arteries, was

optimised for each virtual subject by minimising the absolute difference between the desired and expected carotid-femoral PWV. The desired values were influenced by age and normal variation in MAP and PWV. For the baseline subject at each age (with age-specific baseline values for MAP and PWV), $k_3 \approx 430{,}118 - 1871.3*age + 244.11*age^2$ $gs^{-2}cm^{-1}$.

5.4 Pulse Wave Analysis Algorithms

Pulse wave analysis was performed using the *PulseAnalyse* script (see the Endnote for access). The methods used for detecting each of the fiducial points (see Figure 4) on the pressure and PPG PWs are now described.

PWs were pre-processed by: (i) removing very high frequencies with a low-pass filter with -3 dB cutoff frequency of 16.75 Hz; (ii) removing very low frequencies by subtracting any linear trend between PW onset and end; and (iii) aligning PWs to start at the beginning of the systolic upslope. First, second and third derivatives were calculated using a first derivative Savitzky-Golay filter with a window size of 5 samples (141). The fourth derivative was calculated from the third derivative using a first derivative Savitzky-Golay filter with a window size of 9 samples.

Fiducial points were then identified using the criteria listed in Table A3. These criteria are adapted from (30). PW indices were calculated from these fiducial points as described in (30). The augmentation index and pressure were calculated using *p1in* and *p2pk* (referred to as P1 and P2 in Figure 4). The stiffness index was calculated by assuming a height of 1.75 m, in keeping with (108).

Table A3: The criteria used to identify fiducial points on the pressure and photoplethysmogram (PPG) pulse waves (PWs). Definitions: *x* – PW; *x'* – first derivative of PW; *x''* – second derivative of PW; *x'''* – third derivative of PW; *x''''* – fourth derivative of PW.

Fiducial Point	**Criterion for finding location**
s: systolic peak	Maximum of *x*
ms: maximum slope	Maximum of *x'*
a	The highest local maximum of *x''* between an initial buffer of 0.005 seconds and *ms*. If no local maximum is found in this region then *a* is defined as the last local maximum before the initial buffer.
b	The lowest local minimum of *x''* between *a* and an upper bound of 25% of the PW duration.
p1in	Two candidate locations for *p1in* are identified as: (i) the first local minimum on *x'* after 0.1 s; and (ii) the second local minimum (if it exists, otherwise the first) on *x'* after *b*. *p1in* is taken to be the candidate location which occurs first. If this is later than 0.18 s, then *p1in* is updated to be the first local minimum in *x''''* after 0.1 s. If *p1in* is still later than 0.18 s, then it is updated to be the last local minimum in the first derivative before 0.18 s.
e	A candidate location for *e* is identified as the highest local maximum on *x''* between *ms* and 60% of the PW duration. If this is the first local maximum within this search region, then it may be the *c* point. To check for this, inflection points are identified between *b* and this candidate location (from local minima on *x'''*). If there are no inflection points, and if there is one local maximum in this search region, then update the candidate location to be the first local maximum on *x''* at or after 60% of the PW duration.
c	*c* is identified as the highest local maximum on *x''* between *b* and *e*. If there are no local maxima in this search region, then identify *c* as the lowest local minimum on *x'''* after *b* and before *e*.
dic: dicrotic notch	*dic* is coincident with *e*
dia: diastolic peak	If there is one or more local maxima on *x* after *dic* and before 80% of the PW duration, then take the first local maximum as *dia*. If there isn't, then take the first local maximum on *x'* after *e* and before 80% of the PW duration.
d	*d* is identified as the lowest local minimum on *x''* between *c* and *e*, unless there isn't a local minimum in this search region, in which case take *d* as coincident with *c*.
p2in	A candidate location for *p2in* is taken as the last local minimum on *x'''* before *d*. If this locationis before *p1in*, then it is updated to be the last local minimum on *x'''* before *e*. If there is one or more local maxima on *x* between the candidate location and *e*, then take the last local maximum as *p2in*.
p1pk and *p2pk*	Initial locations of *p1pk* and *p2pk* are set to the locations of *p1in* and *p2in*. Either *p1pk* or *p2pk* is adjusted to be coincident with *sys* (determined by whichever of *p1in* or *p2in* is closest to *sys*). Each of *p1pk* and *p2pk* is then adjusted to be at a nearby local maximum on *x*, if there is a local maximum which satisfies the following criteria. The maximum must lie between the mean of the candidate locations of *p1pk* and *p2pk*, and *ms* for *p1pk*, and *e* for *p2pk*. It must also be higher than the candidate locations. If more than one maximum satisfies these criteria then the maximum with the highest value is taken.

751

752 **Grants**

753 This work was supported by the British Heart Foundation [PG/15/104/31913], the Wellcome
754 EPSRC Centre for Medical Engineering at King's College London [WT 203148/Z/16/Z], and the King's
755 College London & Imperial College London EPSRC Centre for Doctoral Training in Medical Imaging
756 [EP/L015226/1] funding for JMH. The authors acknowledge financial support from the Department
757 of Health through the National Institute for Health Research (NIHR) Cardiovascular MedTech Co-
758 operative at Guy's and St Thomas' NHS Foundation Trust (GSTT). The views expressed are those of
759 the authors and not necessarily those of the BHF, Wellcome Trust, EPSRC, NIHR or GSTT.

760 **Disclosures**

761 No conflicts of interest, financial or otherwise, are declared by the author(s).

762 **ENDNOTE**

763 At the request of the authors, readers are herein alerted to the fact that additional materials
764 related to this manuscript may be found at https://doi.org/10.5281/zenodo.3374476. These
765 materials are not a part of this manuscript, and have not undergone peer review by the American
766 Physiological Society (APS). APS and the journal editors take no responsibility for these materials, for
767 the website address, or for any links to or from it.

768

List of Abbreviations

The following abbreviations are used in this article:

1D – one-dimensional
A – area
AGI_{mod} – modified ageing index
AIx – augmentation index
AP – augmentation pressure
au – arbitrary units
BP – blood pressure
bpm – beats per minute
CO – cardiac output
c_d – diastolic wave speed
CT – crest time
CV – cardiovascular
DBP – diastolic blood pressure
ΔT – time between systolic and diastolic peaks
dia – diastolic peak
Dia – diameter
dic – dicrotic notch
E – Young's modulus
Γ – arterial wall viscosity
H – arterial wall thickness
HR – heart rate
I – relative sensitivity index
LVET – left ventricular ejection time
MAP – mean arterial pressure
MAPE – mean absolute percentage error
ms – point of maximal slope
MRI – magnetic resonance imaging
μ – blood viscosity
P – pressure
P1 – pressure at first shoulder
P2 – pressure at second pressure peak
PFT – peak flow time
PP – pulse pressure
PP_{amp} – pulse pressure amplification
PPG – photoplethysmogram
PTT – pulse transit time
PVC – peripheral vascular compliance
PVR – peripheral vascular resistance
PW – pulse wave
PWV – pulse wave velocity
Q – flow rate
R_d – diastolic arterial radius
ρ – blood density
RFV – reverse flow volume
RI – reflection index
RMS – root mean square
R^2 – coefficient of determination
s – systolic peak
SBP – systolic blood pressure
SD – standard deviation
SI – stiffness index
SV – stroke volume
SVC – systemic vascular compliance
SVR – systemic vascular resistance
T – cardiac period
t_{dia} – duration of diastole
Tr – time to return of the reflected pressure wave
U – flow velocity

References

1. **Agmon Y**, **Khandheria BK**, **Meissner I**, **Schwartz GL**, **Sicks JD**, **Fought AJ**, **O'Fallon WM**, **Wiebers DO**, **Tajik AJ**. Is aortic dilatation an atherosclerosis-related process? Clinical, laboratory, and transesophageal echocardiographic correlates of thoracic aortic dimensions in the population with implications for thoracic aortic aneurysm formation. *J Am Coll Cardiol* 42: 1076–1083, 2003.

2. **Alastruey J**, **Parker K**, **Sherwin S**. Arterial pulse wave haemodynamics. In: *Proc. BHR Group's 11th International Conference on Pressure Surges*. Lisbon, Portugal: 2012, p. 401–443.

3. **Alastruey J**, **Parker KH**, **Peiró J**, **Sherwin SJ**. Can the modified Allen's test always detect sufficient collateral flow in the hand? A computational study. *Comput Methods Biomech Biomed Engin* 9: 353–361, 2006.

4. **Allen J**. Photoplethysmography and its application in clinical physiological measurement. *Physiol Meas* 28: R1–R39, 2007.

5. **Allen J**, **Murray A**. Age-related changes in the characteristics of the photoplethysmographic pulse shape at various body sites. *Physiol Meas* 24: 297–307, 2003.

6. **Aoyama K**, **Emoto T**, **Akutagawa M**, **Masuda M**, **Minato S**, **Obara S**, **Yoshizaki K**, **Kitaoka K**, **Tanaka H**, **Konaka S**, **Kinouchi Y**. Evaluating the atherosclerosis based on blood flow velocity waveform of common carotid artery. *Proc - IEEE-EMBS Int Conf Biomed Heal Informatics Glob Gd Chall Heal Informatics, BHI 2012* 25: 655–658, 2012.

7. **Arora RR**, **Machac J**, **Goldman ME**, **Butler RN**, **Gorlin R**, **Horowitz SF**. Atrial kinetics and left ventricular diastolic filling in the healthy elderly. *J Am Coll Cardiol* 9: 1255–1260, 1987.

8. **Avolio AP**, **Van Bortel LM**, **Boutouyrie P**, **Cockcroft JR**, **McEniery CM**, **Protogerou AD**, **Roman MJ**, **Safar ME**, **Segers P**, **Smulyan H**. Role of pulse pressure amplification in arterial hypertension. *Hypertension* 54: 375–383, 2009.

9. **Avolio AP**, **Chen SG**, **Wang RP**, **Zhang CL**, **Li MF**, **O'Rourke MF**. Effects of aging on changing arterial compliance and left ventricular load in a northern Chinese urban community. *Circulation* 68: 50–58, 1983.

10. **Avolio AP**, **Deng FQ**, **Li WQ**, **Luo YF**, **Huang ZD**, **Xing LF**, **O'Rourke MF**. Effects of aging on arterial distensibility in populations with high and low prevalence of hypertension: comparison between urban and rural communities in China. *Circulation* 71: 202–10, 1985.

11. **Ayer JG**, **Harmer JA**, **Marks GB**, **Avolio A**, **Celermajer DS**. Central arterial pulse wave augmentation is greater in girls than boys, independent of height. *J Hypertens* 28: 306–313, 2010.

12. **Benetos A**, **Adamopoulos C**, **Bureau JM**, **Temmar M**, **Labat C**, **Bean K**, **Thomas F**, **Pannier B**, **Asmar R**, **Zureik M**, **Safar M**, **Guize L**. Determinants of accelerated progression of arterial stiffness in normotensive subjects and in treated hypertensive subjects over a 6-year period. *Circulation* 105: 1202–1207, 2002.

13. **Benetos A**, **Laurent S**, **Hoeks AP**, **Boutouyrie PH**, **Safar ME**. Arterial alterations with aging and high blood pressure. A noninvasive study of carotid and femoral arteries. *Arterioscler Thromb Vasc Biol* 13: 90–97, 1993.

14. **Benetos A**, **Thomas F**, **Joly L**, **Blacher J**, **Pannier B**, **Labat C**, **Salvi P**, **Smulyan H**, **Safar ME**. Pulse pressure amplification. A mechanical biomarker of cardiovascular risk. *J Am Coll Cardiol* 55: 1032–1037, 2010.

15. **Bensalah MZ**, **Bollache E**, **Kachenoura N**, **Giron A**, **De Cesare A**, **Macron L**, **Lefort M**, **Redheuill A**, **Mousseaux E**. Geometry is a major determinant of flow reversal in proximal aorta. *Am J Physiol Heart Circ Physiol* 306: H1408–H1416, 2014.

16. **Bortolotto LA**, **Hanon O**, **Franconi G**, **Boutouyrie P**, **Legrain S**, **Girerd X**. The aging process modifies the distensibility of elastic but not muscular arteries. *Hypertension* 34: 889–892, 1999.

17. **Boss GR**, **Seegmiller JE**. Age-related physiological changes and their clinical significance. *West J Med* 135: 434–40, 1981.

18. **Bramwell JC**, **Hill A V**. Velocity of transmission of the pulse-wave, and elasticity of arteries. *Lancet* 199: 891–2, 1922.

19. **Bramwell JC**, **Hill A V**, **McSwiney BA**. The velocity of the pulse wave in man in relation to age as measured by the hot-wire sphygmograph. *Heart* 10: 233–55, 1923.

20. **Cain PA**, **Ahl R**, **Hedstrom E**, **Ugander M**, **Allansdotter-Johnsson A**, **Friberg P**, **Arheden H**. Age and gender specific normal values of left ventricular mass, volume and function for gradient echo magnetic resonance imaging: a cross sectional study. *BMC Med Imaging* 9: 2, 2009.

21. **Campens L**, **Demulier L**, **De Groote K**, **Vandekerckhove K**, **De Wolf D**, **Roman MJ**, **Devereux RB**, **De Paepe A**, **De Backer J**. Reference values for echocardiographic assessment of the diameter of the aortic root and ascending aorta spanning all age categories. *Am J Cardiol* 114: 914–920, 2015.

22. **Carlsson M**, **Andersson R**, **Bloch K**, **Steding-Ehrenborg K**, **Mosén H**, **Stahlberg F**, **Ekmehag B**, **Arheden H**. Cardiac output and cardiac index measured with cardiovascular magnetic resonance in healthy subjects, elite athletes and patients with congestive heart failure. *J Cardiovasc Magn Reson* 14: 51, 2012.

23. **Charlton P**, **Aresu M**, **Spear J**, **Chowienczyk P**, **Alastruey J**. Indices to assess aortic stiffness from the finger photoplethysmogram: In silico and in vivo testing. *Artery Res* 24: 128, 2018.

24. **Charlton P**, **Chowienczyk P**, **Alastruey J**. An assessment of aortic stiffness indices using a model of healthy cardiovascular ageing, in "Abstracts from the 2018 Annual Scientific Meeting of the British and Irish Hypertension Society (BIHS)." *J Hum Hypertens* 32: 693–721, 2018.

25. **Charlton P**, **Smith J**, **Camporota L**, **Beale R**, **Alastruey J**. Optimising the Windkessel model for cardiac output monitoring during changes in vascular tone. In: *Conf Proc Eng Med Biol Soc.* Chicago, IL: IEEE, 2014, p. 3759–3762.

26. **Charlton PH**. PulseAnalyse: a signal processing tool for cardiovascular pulse waves. Zenodo: http://doi.org/10.5281/zenodo.3272122: 2019.

27. **Charlton PH**, **Birrenkott DA**, **Bonnici T**, **Pimentel MAF**, **Johnson AEW**, **Alastruey J**, **Tarassenko L**, **Watkinson PJ**, **Beale R**, **Clifton DA**. Breathing rate estimation from the electrocardiogram and photoplethysmogram: a review. *IEEE Rev Biomed Eng* 11: 2–20, 2018.

28. **Charlton PH**, **Bonnici T**, **Tarassenko L**, **Alastruey J**, **Clifton DA**, **Beale R**, **Watkinson PJ**. Extraction of respiratory signals from the electrocardiogram and photoplethysmogram: technical and physiological determinants. *Physiol Meas* 38: 669–90, 2017.

29. **Charlton PH**, **Bonnici T**, **Tarassenko L**, **Clifton DA**, **Beale R**, **Watkinson PJ**. An assessment of algorithms to estimate respiratory rate from the electrocardiogram and photoplethysmogram. *Physiol Meas* 37: 610–26, 2016.

30. **Charlton PH**, **Celka P**, **Farukh B**, **Chowienczyk P**, **Alastruey J**. Assessing mental stress from the photoplethysmogram: a numerical study. *Physiol Meas* 39: 054001, 2018.

31. **Charlton PH**, **Mariscal Harana J**, **Vennin S**, **Chowienczyk P**, **Alastruey-Arimon J**. A database for the development of pulse wave analysis algorithms. In: *BioMedEng18 Conference*. London, UK: 2018.

32. **Charlton PH**, **Mariscal Harana J**, **Vennin S**, **Li Y**, **Chowienczyk P**, **Alastruey J**. Pulse Wave Database (PWDB): A database of arterial pulse waves representative of healthy adults. Zenodo: https://doi.org/10.5281/zenodo.2633175: 2019.

33. **Charlton PH**, **Mariscal Harana J**, **Vennin S**, **Li Y**, **Chowienczyk P**, **Alastruey J**. Pulse Wave Database (PWDB) Algorithms. Zenodo: https://doi.org/10.5281/zenodo.3271512: 2019.

34. **Charlton PH**, **Mariscal Harana J**, **Vennin S**, **Willemet M**, **Chowienczyk P**, **Alastruey J**. Modelling arterial pulse wave propagation during healthy ageing. In: *World Congress of Biomechanics 2018*. Dublin, Ireland: 2018.

35. **Chemla D**, **Hébert J-L**, **Coirault C**, **Zamani K**, **Suard I**, **Colin P**, **Lecarpentier Y**. Total arterial compliance estimated by stroke volume-to-aortic pulse pressure ratio in humans. *Am J Physiol Circ Physiol* 274: H500–H505, 1998.

36. **Chen CH**, **Nakayama M**, **Nevo E**, **Fetics BJ**, **Lowell Maughan W**, **Kass DA**. Coupled systolic-ventricular and vascular stiffening with age: Implications for pressure regulation and cardiac reserve in the elderly. *J Am Coll Cardiol* 32: 1221–1227, 1998.

37. **Chirinos JA**, **Kips JG**, **Roman MJ**, **Medina-Lezama J**, **Li Y**, **Woodiwiss AJ**, **Norton GR**, **Yasmin**, **Van Bortel L**, **Wang JG**, **Cockcroft JR**, **Devereux RB**, **Wilkinson IB**, **Segers P**, **McEniery CM**. Ethnic differences in arterial wave reflections and normative equations for augmentation index. *Hypertension* 57: 1108–1116, 2011.

38. **Chowienczyk PJ**, **Kelly RP**, **MacCallum H**, **Millasseau SC**, **Andersson TLG**, **Gosling RG**, **Ritter JM**, **Änggård EE**. Photoplethysmographic assessment of pulse wave reflection: Blunted response to endothelium-dependent beta2-adrenergic vasodilation in type II diabetes mellitus. *J Am Coll Cardiol* 34: 2007–2014, 1999.

39. **Coccarelli A**, **Hasan HM**, **Carson J**, **Parthimos D**, **Nithiarasu P**. Influence of ageing on human body blood flow and heat transfer: A detailed computational modelling study. *Int J Numer Method Biomed Eng* 34: 1–21, 2018.

40. **Craiem D**, **Chironi G**, **Redheuil A**, **Casciaro M**, **Mousseaux E**, **Simon A**, **Armentano RL**. Aging impact on thoracic aorta 3D morphometry in intermediate-risk subjects: looking beyond coronary arteries with non-contrast cardiac CT. *Ann Biomed Eng* 40: 1028–38, 2012.

41. **Dontas AS**, **Taylor HL**, **Keys A**. Carotid pressure plethysmograms. Effects of age, diastolic blood pressure, relative body weight and physical activity. *Arch Kreislaufforsch* 36: 49–58,

953 1961.

954 42. **Dotter CT**, **Roberts DJ**, **Steinberg I**. Aortic length: angiocardiographic measurements.
955 *Circulation* 2: 915–920, 1950.

956 43. **Eliakim M**, **Sapoznikov D**, **Weinman J**. Pulse wave velocity in healthy subjects and in patients
957 with various disease states. *Am Heart J* 82: 448–57, 1971.

958 44. **Epstein S**, **Vergnaud AC**, **Elliott P**, **Chowienczyk P**, **Alastruey J**. Numerical assessment of the
959 stiffness index. In: *Conf Proc IEEE Eng Med Biol Soc.* 2014, p. 1969–1972.

960 45. **Fleg JL**, **O'Connor F**, **Gerstenblith G**, **Becker LC**, **Clulow J**, **Schulman SP**, **Lakatta EG**. Impact of
961 age on the cardiovascular response to dynamic upright exercise in healthy men and women. *J*
962 *Appl Physiol* 78: 890–900, 1995.

963 46. **Flück D**, **Beaudin AE**, **Steinback CD**, **Kumarpillai G**, **Shobha N**, **McCreary CR**, **Peca S**, **Smith EE**,
964 **Poulin MJ**. Effects of aging on the association between cerebrovascular responses to visual
965 stimulation, hypercapnia and arterial stiffness. *Front Physiol* 5: 49, 2014.

966 47. **Folkow B**, **Svanborg A**. Physiology of cardiovascular aging. *Physiol Rev* 73: 725–764, 1993.

967 48. **Freis ED**, **Kyle MC**. Computer analysis of carotid and brachial pulse waves. Effects of age in
968 normal subjects. *Am J Cardiol* 22: 691–695, 1968.

969 49. **Fridericia LS**. The duration of systole in an electrocardiogram in normal humans and in
970 patients with heart disease. *Ann Noninvasive Electrocardiol* 8: 343–51, 2003.

971 50. **Fulton JS**, **McSwiney BA**. The pulse wave velocity and extensibility of the brachial and radial
972 artery in man. *J Physiol* 69: 387–392, 1930.

973 51. **Gaddum N**. TTAlgorithm, available at:
974 http://www.mathworks.co.uk/matlabcentral/fileexchange/37746-ttalgorithm. 2012.

975 52. **Gaddum N**, **Alastruey J**, **Chowienczyk P**, **Rutten MCM**, **Segers P**, **Schaeffter T**. Relative
976 contributions from the ventricle and arterial tree to arterial pressure and its amplification: an
977 experimental study. *Am J Physiol Circ Physiol* 313: H558–H567, 2017.

978 53. **Gaddum NR**, **Alastruey J**, **Beerbaum P**, **Chowienczyk P**, **Schaeffter T**. A technical assessment
979 of pulse wave velocity algorithms applied to non-invasive arterial waveforms. *Ann Biomed*
980 *Eng* 41: 2617–2629, 2013.

981 54. **Gardin JM**, **Davidson DM**, **Rohan MK**, **Butman S**, **Knoll M**, **Garcia R**, **Dubria S**, **Gardin SK**,
982 **Henry WL**. Relationship between age, body size, gender, and blood pressure and Doppler
983 flow measurements in the aorta and pulmonary artery. *Am Heart J* 113: 101–9, 1987.

984 55. **Gerstenblith G**, **Frederiksen J**, **Yin F**, **Fortuin N**, **Lakatta E**, **Weisfeldt M**. Echocardiographic
985 assessment of a normal aging population. *Circulation* 56: 273-278., 1977.

986 56. **Gozna E**, **Marble A**. Age-related changes in the mechanics of the aorta and pulmonary artery
987 of man. *J Appl Physiol* 36: 407–411, 1974.

988 57. **Green DJ**, **Swart A**, **Exterkate A**, **Naylor LH**, **Black MA**, **Cable NT**, **Thijssen DHJ**. Impact of age,
989 sex and exercise on brachial and popliteal artery remodelling in humans. *Atherosclerosis* 210:
990 525–530, 2010.

58. **Greenwald SE**, **Newman DL**. Impulse propagation through junctions. *Med Biol Eng Comput* 20: 343–350, 1982.

59. **Guala A**, **Camporeale C**, **Ridolfi L**. Compensatory effect between aortic stiffening and remodelling during ageing. *PLoS One* 10: 1–14, 2015.

60. **Guala A**, **Camporeale C**, **Ridolfi L**, **Mesin L**. Non-invasive aortic systolic pressure and pulse wave velocity estimation in a primary care setting: An in silico study. *Med Eng Phys* 42: 91–98, 2017.

61. **Guala A**, **Scalseggi M**, **Ridolfi L**. Coronary fluid mechanics in an ageing cardiovascular system. *Meccanica* 52: 503–514, 2017.

62. **Hallock P**. Arterial elasticity in man in relation to age as evaluated by the pulse wave velocity method. *Arch Intern Med* 54: 770, 1934.

63. **Hansen F**, **Mangell P**, **Sonesson B**, **Länne T**. Diameter and compliance in the human common carotid artery - variations with age and sex. *Ultrasound Med Biol* 21: 1–9, 1995.

64. **Harley A**, **Starmer CF**, **Greenfield JC**. Pressure-flow studies in man. An evaluation of the duration of the phases of systole. *J Clin Invest* 48: 895–905, 1969.

65. **Haynes FW**, **Ellis LB**, **Weiss S**. Pulse wave velocity and arterial elasticity in arterial hypertension, arteriosclerosis, and related conditions. *Am Heart J* 11: 385–401, 1936.

66. **van der Heijden-Spek JJ**, **Staessen J a**, **Fagard RH**, **Hoeks a P**, **Boudier H a**, **van Bortel LM**. Effect of age on brachial artery wall properties differs from the aorta and is gender dependent: a population study. *Hypertension* 35: 637–642, 2000.

67. **Hickson SS**, **Butlin M**, **Graves M**, **Taviani V**, **Avolio AP**, **McEniery CM**, **Wilkinson IB**. The relationship of age with regional aortic stiffness and diameter. *JACC Cardiovasc Imaging* 3: 1247–1255, 2010.

68. **Hirata K**, **Yaginuma T**, **O'Rourke MF**, **Kawakami M**. Age-related changes in carotid artery flow and pressure pulses: Possible implications for cerebral microvascular disease. *Stroke* 37: 2552–2556, 2006.

69. **Horváth IG**, **Németh Á**, **Lenkey Z**, **Alessandri N**, **Tufano F**, **Kis P**, **Gaszner B**, **Cziráki A**. Invasive validation of a new oscillometric device (Arteriograph) for measuring augmentation index, central blood pressure and aortic pulse wave velocity. *J Hypertens* 28: 2068–2075, 2010.

70. **Houghton D**, **Jones TW**, **Cassidy S**, **Siervo M**, **MacGowan GA**, **Trenell MI**, **Jakovljevic DG**. The effect of age on the relationship between cardiac and vascular function. *Mech Ageing Dev* 153: 1–6, 2016.

71. **Hughes AD**, **Park C**, **Davies J**, **Francis D**, **McG Thom SA**, **Mayet J**, **Parker KH**. Limitations of augmentation index in the assessment of wave reflection in normotensive healthy individuals. *PLoS One* 8: 1–8, 2013.

72. **Janner JH**, **Godtfredsen NS**, **Ladelund S**, **Vestbo J**, **Prescott E**. Aortic augmentation index: Reference values in a large unselected population by means of the SphygmoCor device. *Am J Hypertens* 23: 180–185, 2010.

73. **Joh JH**, **Ahn HJ**, **Park HC**. Reference diameters of the abdominal aorta and iliac arteries in the

Korean population. *Yonsei Med J* 54: 48–54, 2013.

74. **Kamimura D**, **Hans S**, **Suzuki T**, **Fox ER**, **Hall ME**, **Musani SK**, **McMullan MR**, **Little WC**. Delayed time to peak velocity is useful for detecting severe aortic stenosis. *J Am Heart Assoc* 5: e003907, 2016.

75. **Karamanoglu M**, **Gallagher DE**, **Avolio AP**, **Rourke MF**. Pressure wave propagation of the human upper limb in a multibranched model. *Am J Physiol Heart Circ Physiol* 269: H1363–H1369, 1995.

76. **Kawamoto A**, **Shimada K**, **Matsubayashi K**, **Chikamori T**, **Kuzume O**, **Ogura H**, **Ozawa T**. Cardiovascular regulatory functions in elderly patients with hypertension. *Hypertens (Dallas, Tex 1979)* 13: 401–407, 1989.

77. **Kawano H**, **Yamamoto K**, **Gando Y**, **Tanimoto M**, **Murakami H**, **Ohmori Y**, **Sanada K**, **Tabata I**, **Higuchi M**, **Miyachi M**. Lack of age-related increase in carotid artery wall viscosity in cardiorespiratory fit men. *J Hypertens* 31: 2370–2379, 2013.

78. **Kawel-Boehm N**, **Maceira A**, **Valsangiacomo-Buechel ER**, **Vogel-Claussen J**, **Turkbey EB**, **Williams R**, **Plein S**, **Tee M**, **Eng J**, **Bluemke DA**. Normal values for cardiovascular magnetic resonance in adults and children. *J Cardiovasc Magn Reson* 17: 29, 2015.

79. **Kelly R**, **Hayward C**, **Avolio A**, **Rourke MO**. Noninvasive determination of age-related changes in the human arterial pulse. *Circulation* 80: 1652–1659, 1989.

80. **Kharb S**, **Singh GP**. Distribution of blood viscosity values and biochemical correlates in healthy adults. *J Assoc Physicians India* 47: 505–506, 1999.

81. **Kim J-Y**, **Park J-B**, **Kim D-S**, **Kim K-S**, **Jeong J-W**, **Park J-C**, **Oh B-H**, **Chung N**. Gender difference in arterial stiffness in a multicenter cross-sectional study: The Korean Arterial Aging Study (KAAS). *Pulse* 2: 11–17, 2014.

82. **Kim M**, **Roman MJ**, **Cavallini MC**, **Schwartz JE**, **Pickering TG**, **Devereux RB**. Effect of hypertension on aortic root size and prevalence of aortic regurgitation. *Hypertension* 28: 47–52, 1996.

83. **Kostis JB**, **Moreyra a E**, **Amendo MT**, **Di Pietro J**, **Cosgrove N**, **Kuo PT**. The effect of age on heart rate in subjects free of heart disease. *Circulation* 65: 141–145, 1982.

84. **Lakatta EG**. Cardiovascular regulatory mechanisms in advanced age. *Physiol Rev* 73: 413–67, 1993.

85. **Lakatta EG**. Age-associated cardiovascular changes in health: impact on cardiovascular disease in older persons. *Hear Fail* 7: 29–49, 2002.

86. **Lakatta EG**, **Mitchell JH**, **Pomerance A**, **Rowe GG**. Human aging: Changes in structure and function. *J Am Coll Cardiol* 10: 42A-47A, 1987.

87. **Landowne M**. The relation between intra-arterial pressure and impact pulse wave velocity with regard to age and arteriosclerosis. *J Gerontol* 13: 153–62, 1958.

88. **Langenberg C**, **Hardy R**, **Kuh D**, **Wadsworth ME**. Influence of height, leg and trunk length on pulse pressure, systolic and diastolic blood pressure. *J Hypertens* 21: 537–43, 2003.

89. **Le T-T**, **Tan RS**, **De Deyn M**, **Goh EPC**, **Han Y**, **Leong BR**, **Cook SA**, **Chin CW**. Cardiovascular magnetic resonance reference ranges for the heart and aorta in Chinese at 3T. *J Cardiovasc Magn Reson* 18: 21, 2016.

90. **Li Y**, **Gu H**, **Fok H**, **Alastruey J**, **Chowienczyk P**. Forward and backward pressure waveform morphology in hypertension. *Hypertension* 69: 375–381, 2017.

91. **Li Y**, **Jiang B**, **Keehn L**, **Gu H**, **Boguslavskyi A**, **Cecelja M**, **Vennin S**, **Spector T**, **Alastruey J**, **Chowienczyk P**. Hemodynamic mechanism of the age-related increase in pulse pressure in women. *Hypertension* 73: 1018–1024, 2019.

92. **Liang Y-L**, **Teede H**, **Kotsopoulos D**, **Shiel L**, **Cameron JD**, **Dart AM**, **McGrath BP**. Non-invasive measurements of arterial structure and function: repeatability, interrelationships and trial sample size. *Clin Sci* 95: 669–679, 1998.

93. **Liljestrand G**, **Zander E**. Vergleichende bestimmungen des minutenvolumens des herzens beim menschen mittels der stickoxydulmethode und durch blutdruckmessung. *Z Gesamte Exp Med* 59: 105–122, 1928.

94. **López-Beltrán E a**, **Blackshear PL**, **Finkelstein SM**, **Cohn JN**. Non-invasive studies of peripheral vascular compliance using a non-occluding photoplethysmographic method. *Med Biol Eng Comput* 36: 748–753, 1998.

95. **Maksuti E**, **Westerhof N**, **Westerhof BE**, **Broomé M**, **Stergiopulos N**. Contribution of the arterial system and the heart to blood pressure during normal aging - A simulation study. *PLoS One* 11: 1–12, 2016.

96. **Mangoni a a**, **Kinirons MT**, **Swift CG**, **Jackson SH**. Impact of age on QT interval and QT dispersion in healthy subjects: a regression analysis. *Age Ageing* 32: 326–331, 2003.

97. **Mao SS**, **Ahmadi N**, **Shah B**, **Beckmann D**, **Chen A**, **Ngo L**, **Flores FR**, **Gao Y lin**, **Budoff MJ**. Normal thoracic aorta diameter on cardiac computed tomography in healthy asymptomatic adults. Impact of age and gender. *Acad Radiol* 15: 827–834, 2008.

98. **Mattace-Raso FUS**, **Hofman A**, **Verwoert GC**, **Wittemana JCM**, **Wilkinson I**, **Cockcroft J**, **McEniery C**, **Yasmina**, **Laurent S**, **Boutouyrie P**, **Bozec E**, **Hansen TW**, **Torp-Pedersen C**, **Ibsen H**, **Jeppesen J**, **Vermeersch SJ**, **Rietzschel E**, **de Buyzere M**, **Gillebert TC**, **van Bortel L**, **Segers P**, **Vlachopoulos C**, **Aznaouridis C**, **Stefanadis C**, **Benetos A**, **Labat C**, **Lacolley P**, **Stehouwer CDA**, **Nijpels G**, **Dekker JM**, **Ferreira I**, **Twisk JWR**, **Czernichow S**, **Galan P**, **Hercberg S**, **Pannier B**, **Guérin A**, **London G**, **Kennedy Cruickshank J**, **Anderson SG**, **Paini A**, **Rosei EA**, **Muiesan ML**, **Salvetti M**, **Filipovsky J**, **Seidlerova J**, **Dolejsova M**. Determinants of pulse wave velocity in healthy people and in the presence of cardiovascular risk factors: 'Establishing normal and reference values.' *Eur Heart J* 31: 2338–2350, 2010.

99. **McEniery CM**, **Wilkinson IB**, **Avolio AP**. Age, hypertension and arterial function. *Clin Exp Pharmacol Physiol* 34: 665–671, 2007.

100. **McEniery CM**, **Yasmin**, **Hall IR**, **Qasem A**, **Wilkinson IB**, **Cockcroft JR**. Normal vascular aging: Differential effects on wave reflection and aortic pulse wave velocity - The Anglo-Cardiff Collaborative Trial (ACCT). *J Am Coll Cardiol* 46: 1753–1760, 2005.

101. **McVeigh GE**, **Bratteli CW**, **Morgan DJ**, **Alinder CM**, **Glasser SP**, **Finkelstein SM**, **Cohn JN**. Age-related abnormalities in arterial compliance identified by pressure pulse contour analysis:

aging and arterial compliance. *Hypertension* 33: 1392–1398, 1999.

102. **Medical Services Advisory Committee**. *Peripheral arterial tonometry with ascending aortic waveform analysis using the SphygmoCor system*. 2006.

103. **Merillon JP**, **Motte G**, **Masquet C**, **Azancot I**, **Guiomard A**, **Gourgonf R**. Relationship between physical properties of the arterial system and left ventricular performance in the course of aging and arterial hypertension. *Eur Heart J* 3: 95–102, 1982.

104. **Merri M**, **Benhorin J**, **Alberti M**, **Locati E**, **Moss AJ**. Electrocardiographic quantitation of ventricular repolarization. *Circulation* 80: 1301–8, 1989.

105. **Millasseau SC**, **Kelly RP**, **Ritter JM**, **Chowienczyk PJ**. Determination of age-related increases in large artery stiffness by digital pulse contour analysis. *Clin Sci* 103: 371–377, 2002.

106. **Millasseau SC**, **Stewart AD**, **Patel SJ**, **Redwood SR**, **Chowienczyk PJ**. Evaluation of carotid-femoral pulse wave velocity: Influence of timing algorithm and heart rate. *Hypertension* 45: 222–226, 2005.

107. **Mitchell GF**, **Parise H**, **Benjamin EJ**, **Larson MG**, **Keyes MJ**, **Vita JA**, **Vasan RS**, **Levy D**. Changes in arterial stiffness and wave reflection with advancing age in healthy men and women: The Framingham Heart Study. *Hypertension* 43: 1239–1245, 2004.

108. **Mynard JP**, **Smolich JJ**. One-dimensional haemodynamic modeling and wave dynamics in the entire adult circulation. *Ann Biomed Eng* 43: 1443–1460, 2015.

109. **Nichols WW**, **O'Rourke MF**, **Avolio AP**, **Yaginuma T**, **Murgo JP**, **Pepine CJ**, **Conti CR**. Effects of age on ventricular-vascular coupling. *Am J Cardiol* 55: 1179–1184, 1985.

110. **O'Rourke MF**. Arterial aging: pathophysiological principles. *Vasc Med* 12: 329–41, 2007.

111. **O'Rourke MF**. Time domain analysis of the arterial pulse in clinical medicine. *Med Biol Eng Comput* 47: 119–129, 2009.

112. **O'Rourke MF**, **Blazek J V**, **Morreels CL**, **Krovetz LJ**. Pressure wave transmission along the human aorta. *Circ Res* 23: 567–579, 1968.

113. **O'Rourke MF**, **Hashimoto J**. Mechanical factors in arterial aging. A clinical perspective. *J Am Coll Cardiol* 50: 1–13, 2007.

114. **Olufsen MS**. Structured tree outflow condition for blood flow in larger systemic arteries. In: *Am J Physiol*. 1999, p. H257–H268.

115. **Pagoulatou S**, **Stergiopulos N**. Evolution of aortic pressure during normal ageing: A model-based study. *PLoS One* 12: 1–14, 2017.

116. **Papaioannou TG**, **Vardoulis O**, **Stergiopulos N**. The "systolic volume balance" method for the noninvasive estimation of cardiac output based on pressure wave analysis. *Am J Physiol Heart Circ Physiol* 302: H2064-73, 2012.

117. **Pauca AL**, **O'Rourke MF**, **Kon ND**. Prospective evaluation of a method for estimating ascending aortic pressure from the radial artery pressure waveform. *Hypertension* 38: 932–937, 2001.

118. **Pedersen OM**, **Aslaksen A**, **Vik-Mo H**. Ultrasound measurement of the luminal diameter of

the abdominal aorta and iliac arteries in patients without vascular disease. *J Vasc Surg* 17: 596–601, 1993.

119. **Petersen SE**, **Aung N**, **Sanghvi MM**, **Zemrak F**, **Fung K**, **Paiva JM**, **Francis JM**, **Khanji MY**, **Lukaschuk E**, **Lee AM**, **Carapella V**, **Kim YJ**, **Leeson P**, **Piechnik SK**, **Neubauer S**. Reference ranges for cardiac structure and function using cardiovascular magnetic resonance (CMR) in Caucasians from the UK Biobank population cohort. *J Cardiovasc Magn Reson* 19: 18, 2017.

120. **Pontoriero AD**, **Charlton PH**, **Alastruey J**. Alzheimer's disease: A step towards prognosis using smart wearables. *Proceedings* 4: 8, 2019.

121. **Poppe KK**, **Doughty RN**, **Gardin JM**, **Nagueh SF**, **Whalley GA**, **Cameron V**, **Chadha DS**, **Chien KL**, **Detrano R**, **Akif Duzenli M**, **Ezekowitz J**, **Di Pasquale P**, **Mogelvang R**, **Altman DG**, **Perera R**, **Triggs CM**, **Au Yeung H**, **Beans Picón GA**, **Anderson T**, **Dyck J**, **Ezekowitz JA**, **Chirinos JA**, **De Buyzere ML**, **Gillebert TC**, **Rietzschel E**, **Segers P**, **Van daele CM**, **Walsh HA**, **Whalley GA**, **Izzo R**, **De Luca N**, **Trimarco B**, **De Simone G**, **Chadha DS**, **Goel K**, **Misra A**, **Chen PC**, **Chien KL**, **Lin HJ**, **Su TC**, **Detrano R**, **Richards AM**, **Troughton R**, **Mogelvang R**, **Skov Jensen J**, **Di Pasquale P**, **Paterna S**, **Akif Duzenli M**, **Hobbs FDR**, **Davies MK**, **Davis RC**, **Roalfe A**, **Calvert M**, **Freemantle N**, **Gill PS**, **Lip GYH**, **Kuznetsova T**, **Staessen JA**, **Dargie HJ**, **Ford I**, **McDonagh TA**, **McMurray JJV**, **Grossman E**, **Galasko G**, **Lahiri A**, **Senior R**, **Brown A**, **Carrington M**, **Krum H**, **McGrady M**, **Stewart S**, **Zeitz C**, **Stewart S**, **Blauwet L**, **Sliwa K**, **Dalen H**, **Moelmen Hansen HE**, **Støylen A**, **Thorstensen A**, **Daimon M**, **Watanabe H**, **Yoshikawa J**, **Fukuda S**, **Kim HK**, **Leung NKW**, **Linhart A**, **Senior R**, **Chahal N**, **Chambers JC**, **Kooner J**, **Davies J**, **Loke I**, **Ng L**, **Squire IB**, **Aune E**, **Otterstad JE**, **Leung DY**, **Ng ACT**, **Ojji D**, **Arnold L**, **Coffey S**, **D'Arcy J**, **Hammond C**, **Mabbett C**, **Lima C**, **Loudon M**, **Pinheiro N**, **Prendergast B**, **Reynolds R**, **Badano LP**, **Muraru D**, **Peluso D**, **Petrovic DJ**, **Petrovic J**, **Schvartzman P**, **Fuchs FD**, **Katova T**, **Simova I**, **Kaku K**, **Takeuchi M**, **Boyd A**, **Chia EM**, **Thomas L**, **Schirmer H**, **Angelo LC**, **Pereira AC**, **Krieger JE**, **Mill JG**, **Rodrigues SL**, **Muiesan ML**, **Paini A**, **Agabiti Rosei E**, **Salvetti M**. Ethnic-specific normative reference values for echocardiographic LA and LV Size, LV Mass, and systolic function: The EchoNoRMAL study. *JACC Cardiovasc Imaging* 8: 656–665, 2015.

122. **Proper R**, **Wall F**. Left ventricular stroke volume measurements not affected by chronologic aging. *Am Heart J* 83: 843–845, 1972.

123. **Protogerou AD**, **Blacher J**, **Mavrikakis M**, **Lekakis J**, **Safar ME**. Increased pulse pressure amplification in treated hypertensive subjects with metabolic syndrome. *Am J Hypertens* 20: 127–133, 2007.

124. **Reant P**, **Dijos M**, **Donal E**, **Mignot A**, **Ritter P**, **Bordachar P**, **Dos Santos P**, **Leclercq C**, **Roudaut R**, **Habib G**, **Lafitte S**. Systolic time intervals as simple echocardiographic parameters of left ventricular systolic performance: Correlation with ejection fraction and longitudinal two-dimensional strain. *Eur J Echocardiogr* 11: 834–844, 2010.

125. **Reardon M**, **Malik M**. QT interval change with age in an overtly healthy older population. *Clin Cardiol* 19: 949–52, 1996.

126. **Redfield MM**, **Jacobsen SJ**, **Borlaug BA**, **Rodeheffer RJ**, **Kass DA**. Age- and gender-related ventricular-vascular stiffening: A community-based study. *Circulation* 112: 2254–2262, 2005.

127. **Redheuil A**, **Yu WC**, **Mousseaux E**, **Harouni AA**, **Kachenoura N**, **Wu CO**, **Bluemke D**, **Lima JAC**. Age-related changes in aortic arch geometry: Relationship with proximal aortic function and left ventricular mass and remodeling. *J Am Coll Cardiol* 58: 1262–1270, 2011.

128. **Redheuil A**, **Yu WC**, **Wu CO**, **Mousseaux E**, **De Cesare A**, **Yan R**, **Kachenoura N**, **Bluemke D**, **Lima JAC**. Reduced ascending aortic strain and distensibility: Earliest manifestations of vascular aging in humans. *Hypertension* 55: 319–326, 2010.

129. **Reneman RS**, **van Merode T**, **Hick P**, **Muytjens AM**, **Hoeks AP**. Age-related changes in carotid artery wall properties in men. *Ultrasound Med Biol* 12: 465–71, 1986.

130. **Resnick LM**, **Militianu D**, **Cunnings AJ**, **Pipe JG**, **Evelhoch JL**, **Soulen RL**, **Lester MA**. Pulse waveform analysis of arterial compliance: relation to other techniques, age, and metabolic variables. *Am J Hypertens* 13: 1243–1249, 2000.

131. **Roccabianca S**, **Figueroa CA**, **Tellides G**, **Humphrey JD**. Quantification of regional differences in aortic stiffness in the aging human. *J Mech Behav Biomed Mater* 29: 618–634, 2014.

132. **Rodeheffer RJ**, **Gerstenblith G**, **Beard E**, **Fleg JL**, **Becker LC**, **Weisfeldt ML**, **Lakatta EG**. Postural changes in cardiac volumes in men in relation to adult age. *Exp Gerontol* 21: 367–378, 1986.

133. **Rodeheffer RJ**, **Gerstenblith G**, **Becker LC**, **Fleg JL**, **Weisfeldt ML**, **Lakatta EG**. Exercise cardiac output is maintained with advancing age in healthy human subjects: cardiac dilatation and increased stroke volume compensate for a diminished heart rate. *Circulation* 69: 203–213, 1984.

134. **Rylski B**, **Desjardins B**, **Moser W**, **Bavaria JE**, **Milewski RK**. Gender-related changes in aortic geometry throughout life. *Eur J Cardio-thoracic Surg* 45: 805–811, 2014.

135. **Safar M**. Ageing and its effects on the cardiovascular system. *Drugs* 39: 1–8, 1990.

136. **Sagie A**, **Larson MG**, **Goldberg RJ**, **Bengtson JR**, **Levy D**. An improved method for adjusting the QT interval for heart rate (the Framingham Heart Study). *Am J Cardiol* 70: 797–801, 1992.

137. **Salvi P**, **Grillo A**, **Tan I**, **Simon G**, **Salvi L**, **Gao L**, **Rovina M**, **Butlin M**, **Yang Y**, **Meneghin E**, **Meng L**, **Faini A**, **Barin E**, **Pini A**, **Carretta R**, **Huo Y**, **Avolio A**, **Parati G**. Systolic time intervals assessed from analysis of the carotid pressure waveform. *Physiol Meas* 39: 084002, 2018.

138. **Salvi P**, **Palombo C**, **Salvi GM**, **Labat C**, **Parati G**, **Benetos A**. Left ventricular ejection time, not heart rate, is an independent correlate of aortic pulse wave velocity. *J Appl Physiol* 115: 1610–1617, 2013.

139. **Sandgren T**, **Sonesson B**, **Ahlgren ÅR**, **Länne T**. The diameter of the common femoral artery in healthy human: Influence of sex, age, and body size. *J Vasc Surg* 29: 503–510, 1999.

140. **Sass C**, **Herbeth B**, **Chapet O**, **Siest G**, **Visvikis S**, **Zannad F**. Intima-media thickness and diameter of carotid and femoral arteries in children, adolescents and adults from the Stanislas cohort: Effect of age, sex, anthropometry and blood pressure. *J Hypertens* 16: 1593–1602, 1998.

141. **Savitzky A**, **Golay M**. Smoothing and differentiation of data by simplified least squares procedures. *Anal Chem* 36: 1627–1639, 1964.

142. **Schwartz JB**, **Gibb WJ**, **Tran T**. Aging effects on heart rate variation. *J Gerontol Med Sci* 46: 99–6, 1991.

143. **Scuteri A**, **Morrell CH**, **Orrù M**, **Strait JB**, **Tarasov K V.**, **Ferreli LAP**, **Loi F**, **Pilia MG**, **Delitala A**,

Spurgeon H, **Najjar SS**, **Alghatrif M**, **Lakatta EG**. Longitudinal perspective on the conundrum of central arterial stiffness, blood pressure, and aging. *Hypertension* 64: 1219–1227, 2014.

144. **Segers P**, **Mahieu D**, **Kips J**, **Rietzschel E**, **De Buyzere M**, **De Bacquer D**, **Bekaert S**, **De Backer G**, **Gillebert T**, **Verdonck P**, **Van Bortel L**. Amplification of the pressure pulse in the upper limb in healthy, middle-aged men and women. *Hypertension* 54: 414–420, 2009.

145. **Shaw DJ**, **Rothbaum DA**, **Angell CS**, **Shock NW**. The effects of age and blood pressure upon the systolic time intervals in males aged 20-89 years. *J Gerontol* 28: 133–139, 1973.

146. **Shi Y**, **Lawford P**, **Hose R**. Review of zero-D and 1-D models of blood flow in the cardiovascular system. *Biomed Eng Online* 10: 33, 2011.

147. **Simonson E**, **Nakagawa K**. Effect of age on pulse wave velocity and "aortic ejection time" in healthy men and in men with coronary artery disease. *Circulation* 22: 126–129, 1960.

148. **Simpson DM**, **Wicks R**. Spectral analysis of heart rate indicates reduced baroreceptor-related heart rate variability in elderly persons. *J Gerontol* 43: M21–M24, 1988.

149. **Smulyan H**, **Csermely TJ**, **Mookherjee S**, **Warner RA**. Effect of age on arterial distensibility in Asymptomatic humans. *Arterioscler Thromb Vasc Biol* 3: 199–205, 1983.

150. **Sonesson B**, **Hansen F**, **Stale H**, **Länne T**. Compliance and diameter in the human abdominal aorta - the influence of age and sex. *Eur J Vasc Surg* 7: 690–697, 1993.

151. **Stergiopulos N**, **Westerhof BE**, **Westerhof N**. Physical basis of pressure transfer from periphery to aorta: a model-based study. *Am J Physiol Circ Physiol* 274: H1386–H1392, 1998.

152. **Sugawara J**, **Hayashi K**, **Yokoi T**, **Tanaka H**. Age-associated elongation of the ascending aorta in adults. *JACC Cardiovasc Imaging* 1: 739–748, 2008.

153. **Sun JX**, **Reisner AT**, **Saeed M**, **Mark RG**. Estimating cardiac output from arterial blood pressure waveforms: a critical evaluation using the MIMIC II database. In: *Proc CinC.* IEEE, 2005, p. 295–298.

154. **Svedlund S**, **Wetterholm R**, **Volkmann R**, **Caidahl K**. Retrograde blood flow in the aortic arch determined by transesophageal Doppler ultrasound. *Cerebrovasc Dis* 27: 22–28, 2009.

155. **Taneja T**, **Mahnert BW**, **Passman R**, **Goldberger J**, **Kadish A**. Effects of sex and age on electrocardiographic and cardiac electrophysiological properties in adults. *Pacing Clin Electrophysiol* 24: 16–21, 2001.

156. **Tarassenko L**, **Topol EJ**. Monitoring jet engines and the health of people. *JAMA* 320: 2309, 2018.

157. **Trachet B**, **Reymond P**, **Kips J**, **Swillens A**, **De Buyzere M**, **Suys B**, **Stergiopulos N**, **Segers P**. Numerical validation of a new method to assess aortic pulse wave velocity from a single recording of a brachial artery waveform with an occluding cuff. *Ann Biomed Eng* 38: 876–888, 2010.

158. **Turkbey EB**, **Jain A**, **Johnson C**, **Redheuil A**, **Arai AE**, **Gomes AS**, **Carr J**, **Hundley WG**, **Teixido-Tura G**, **Eng J**, **Lima JAC**, **Bluemke DA**. Determinants and normal values of ascending aortic diameter by age, gender, and race/ethnicity in the Multi-Ethnic Study of Atherosclerosis (MESA). *J Magn Reson Imaging* 39: 360–368, 2014.

159. **Ushiroyama T**, **Kajimoto Y**, **Sakuma K**, **Minoru U**. Assessment of chilly sensation in Japanese women with lasor Doppler fluxmetry and acceleration plethysmogram with respect to peripheral circulation. *Bull Osaka Med Coll* 51: 76–84, 2005.

160. **Vaitkevicius P V.**, **Fleg JL**, **Engel JH**, **O'Connor FC**, **Wright JG**, **Lakatta LE**, **Yin FC**, **Lakatta EG**. Effects of age and aerobic capacity on arterial stiffness in healthy adults. *Circulation* 88: 1456–1462, 1993.

161. **Vennin S**, **Li Y**, **Willemet M**, **Fok H**, **Gu H**, **Charlton P**, **Alastruey J**, **Chowienczyk P**. Identifying hemodynamic determinants of pulse pressure: a combined numerical and physiological approach. *Hypertension* 70: 1176–1182, 2017.

162. **Virmani R**, **Avolio AP**, **Mergner WJ**, **Robinowitz M**, **Herderick EE**, **Cornhill JF**, **Guo SY**, **Liu TH**, **Ou DY**, **O'Rourke M**. Effect of aging on aortic morphology in populations with high and low prevalence of hypertension and atherosclerosis. Comparison between occidental and Chinese communities. *Am J Pathol* 139: 1119–29, 1991.

163. **Vriz O**, **Driussi C**, **Bettio M**, **Ferrara F**, **D'Andrea A**, **Bossone E**. Aortic root dimensions and stiffness in healthy subjects. *Am J Cardiol* 112: 1224–1229, 2013.

164. **Wei CC**. Developing an effective arterial stiffness monitoring system using the spring constant method and photoplethysmography. *IEEE Trans Biomed Eng* 60: 151–154, 2013.

165. **Weissler AM**, **Harris WS**, **Schoenfeld CD**. Systolic time intervals in heart failure in man. *Circulation* 37: 149–159, 1968.

166. **Weissler AM**, **Peeler RG**, **Roehll WH**. Relationships between left ventricular ejection time, stroke volume, and heart rate in normal individuals and patients with cardiovascular disease. *Am Heart J* 62: 367–378, 1961.

167. **Wilkinson IB**, **Franklin SS**, **Hall IR**, **Tyrrell S**, **Cockcroft JR**. Pressure amplification explains why pulse pressure Is unrelated to risk in young subjects. *Hypertension* 38: 1461–1466, 2001.

168. **Wilkinson IB**, **Mohammad NH**, **Tyrrell S**, **Hall IR**, **Webb DJ**, **Paul VE**, **Levy T**, **Cockcroft JR**. Heart rate dependency of pulse pressure amplification and arterial stiffness. *Am J Hypertens* 15: 24–30, 2002.

169. **Wilkinson IB**, **Mohammad NH**, **Tyrrell S**, **Hall IR**, **Webb DJ**, **Paul VE**, **Levy T**, **Cockcroft JR**. Heart rate dependency of pulse pressure amplification and arterial stiffness. *Am J Hypertens* 15: 24–30, 2002.

170. **Willemet M**, **Chowienczyk P**, **Alastruey J**. A database of virtual healthy subjects to assess the accuracy of foot-to-foot pulse wave velocities for estimation of aortic stiffness. *Am J Physiol Heart Circ Physiol* 309: H663-75, 2015.

171. **Willemet M**, **Vennin S**, **Alastruey J**. Computational assessment of hemodynamics-based diagnostic tools using a database of virtual subjects: Application to three case studies. *J Biomech* 49: 3908–3914, 2016.

172. **Willems JL**, **Roelandt J**, **De Geest H**, **Kesteloot H**, **Joossens J V.** The left ventricular ejection time in elderly subjects. *Circulation* 42: 37–42, 1970.

173. **Xu L**, **Liang F**, **Zhao B**, **Wan J**, **Liu H**. Influence of aging-induced flow waveform variation on hemodynamics in aneurysms present at the internal carotid artery: A computational model-

based study. *Comput Biol Med* 101: 51–60, 2018.

174. **Yashin AI**, **Akushevich I V.**, **Arbeev KG**, **Akushevich L**, **Ukraintseva S V.**, **Kulminski A**. Insights on aging and exceptional longevity from longitudinal data: Novel findings from the Framingham heart study. *Age (Omaha)* 28: 363–374, 2006.

175. **Younis LT**, **Melin JA**, **Robert AR**, **Detry JMR**. Influence of age and sex on left ventricular volumes and ejection fraction during upright exercise in normal subjects. *Eur Heart J* 11: 916–924, 1990.

176. **Zhang J**, **Critchley LAH**, **Huang L**. Five algorithms that calculate cardiac output from the arterial waveform: a comparison with Doppler ultrasound. *Br J Anaesth* 115: 1–11, 2015.